Investigation and Application of pH-Sensitive Materials as Sensing Elements in Optical Fibre pH-Sensor Systems

By

Mari Helle Mossestad

Faculty of Mathematics and Natural sciences

Master Thesis in Chemistry

University of Bergen, June 2024

Sammendrag

Denne masteroppgaven utforsker pH-følsomme materialer som kan brukes som sensorelementer i optiske fiber pH-sensorer. Med dette formålet undersøkes to tilnærminger. Den første tilnærmingen omhandler utvikling av en optisk fiber pH-sensor basert på fluorescenslevetiden til akridin. Segmenter av det ytterste belegget (nylon) på en plastkledd kvartsfiber ble fjernet ved hjelp av kokende propylenglykol. Silikonlaget under ble deretter dopet med akridin. Tre dopingprosesser ble overvåket med et optisk kraftmeter. Optiske kraftmålinger ble utført på både dopede og ikke-dopede kabler, både i luft og i Carmody-bufferløsninger med pH-verdier fra 4 til 9. Statistiske tester med et signifikansnivå på 5 % viste signifikante forskjeller i transmisjonsverdier mellom dopet fiber i luft og dopet fiber i Carmody-løsninger fra pH 4 til 9. Ved pH 5 var gjennomsnittssignalet signifikant høyere enn i pH 4. Mellom pH 5 til 6, 6 til 7, 7 til 8, og 8 til 9 ble gjennomsnittssignalene ikke funnet å være signifikant forskjellige. Gjennomsnittssignalet ved pH 4 var signifikant lavere enn gjennomsnittssignalene ved pH 7, 8 og 9. Også gjennomsnittssignalene ved pH 5 og 7 var signifikant lavere enn gjennomsnittssignalet ved pH 9. Og gjennomsnittssignalet ved pH 6 var signifikant lavere enn ved pH 8 og 9.

Den andre tilnærmingen undersøker pH-responsen til utvalgte hydrogeler, som er ment å indusere strekk i en strekkbasert optisk fiber pH-sensor. Disse hydrogelene varierer i total monomerkonsentrasjon, kryssbinderkonsentrasjon og degasseringsmetode, men består alle av ko-monomerene akrylsyre og N-isopropylakrylamid, krysslinkeren N,N'-metylenbisakrylamid og polymeriseringsinitiatorene ammoniumpersulfat og N,N,N',N'-tetrametyletyl-1,2-diamin. pH-responsen til hydrogelene ble undersøkt ved vektbasert beregning av svellingskapasitet i Carmody-bufferløsninger med pH-verdier fra 4 til 9. Prøver fra batch 1 og 2 viste tendenser til pH-sensitivitet i pH-området fra 4 til 7. Statistiske tester fant imidlertid at disse tendensene ikke var signifikant forskjellige, bortsett fra svellingskapasiteten beregnet ved pH 4 sammenlignet med svellingskapasitetene i de andre pH-miljøene.

Av de to tilnærmingene som er undersøkt, viser pH-sensoren basert på fluorescenslevetiden til akridin seg å være den mest lovende for videre undersøkelser. Fremtidige forsøk bør

utforske variasjonen i fluorescens og fluorescenslevetid for akridin i ulike pH-miljøer. For hydrogel-sensorsystemet bør fremtidige eksperimenter forbedre egenskapene til hydrogelene, for eksempel ved å optimalisere kryssbinderkonsentrasjonen. Adhesjonen mellom hydrogelen og ytterkappen på optiske fiberkabler bør også undersøkes i videre eksperiment.

Abstract

The aim of this master's thesis is to explore pH-sensitive materials for use as sensing elements in optical fiber pH-sensor systems. Two routes of applying sensing elements are investigated. The first route explores the development of an optical fibre pH-sensor based on the fluorescence lifetime of acridine. Segments of the coating-material (nylon) on a plastic-clad silica fibre were removed using boiling propylene glycol. The silicone layer underneath was then doped with acridine. Three doping processes were monitored using an optical power monitor. Optical power measurements were conducted on both doped and undoped fibres, in air and in Carmody buffer solutions with pH-values ranging from 4 to 9. Statistical tests with a significance level of 5% determined significant differences in transmission values between doped fibre in air and doped fiber in Carmody solutions from pH 4 to 9. At pH 5, the average signal was significantly higher than at pH 4. Between pH 5 to 6, 6 to 7, 7 to 8, and 8 to 9, the average signals were not found to be significantly different. The average signal at pH 4 was significantly lower than the average signals at pH 7, 8, and 9. Additionally, the average signals at pH 5 and 7 were significantly lower than the average signal at pH 9. And the average signal at pH 6 was significantly lower than at pH 8 and 9.

The second route investigates the pH-response of selected hydrogels, which are intended to induce strain in a strain-based optical fiber pH-sensor system. These hydrogels vary in total monomer concentration, crosslinker concentration, and method of degasification. All hydrogels consist of acrylic acid and N-isopropylacrylamide as comonomers, N,N'-methylenebisacrylamide as crosslinker, and ammonium persulfate and N,N,N',N'-tetramethylethylenediamine as polymerization initiators. The pH response of the hydrogels was examined through weight-based calculation of swelling capacity in Carmody buffer solutions ranging from pH 4 to 9. Samples from batch 1 and 2 showed trends of pH sensitivity in the pH range from 4 to 7. However, statistical tests found that these trends were not statistically significant, except for the swelling capacities measured at pH 4 compared to the other pH environments.

Of the two routes investigated, the pH-sensor based on the fluorescence lifetime of acridine is the most promising for further investigation. Future experiments should explore the

variation in fluorescence and fluorescence lifetime for acridine in different pH-environments. For the hydrogel sensor system, future experiments should improve the properties of the hydrogels, for example by optimizing the crosslinker concentration. The adhesion between the hydrogel and the outer coating of optical fiber cables should also be investigated in further experiments.

Acknowledgements

The experimental work for this master's thesis was conducted in laboratories at the Norwegian Research Centre (NORCE) and the Department of Chemistry at the University of Bergen.

First and foremost, I would like to thank my supervisors, Tore Skodvin and Peter Thomas. Thank you to my main supervisor, Tore, for your support and guidance throughout the completion of this thesis. And thank you, Peter, for your guidance, thoughts, and discussions. You both were most appreciated.

Thank you, Giovanni Occhipinti, for introduction, instructions, and support with the Schlenk line. Thank you to my 2023 summer colleagues at the Department of Measurement Science at NORCE for including me in a productive environment of learning and curiosity. Thank you, Adam Funnell, for research and discussions. Thank you to my fellow master students both at NORCE and the Department of Chemistry for friendships and support through this somewhat stressful period of our lives. Last, but not least, I would like to thank my family and friends for their support and encouragement.

Abbreviations

DCS	Distributed chemical sensing
PCS	Plastic-clad silica
OFC	Optical fibre cable
FL	Fluorescence lifetime
Aac	Acrylic acid
NIPAM	N-isopropylacrylamide
APS	Ammonium persulfate
TEMED	N,N,N′,N′-tetramethylethyl-1,2-diamine
BIS	N,N’-methylenebisacrylamide
SC	Swelling capacity

Table of Contents

1. Introduction

The introduction chapter offers an overview of the background of the thesis and the value of exploring the potential of distributed optical fibre pH-sensors. Relevant research and theory are presented here, alongside the purpose- and goals of the thesis.

1.1 Background

The hydrogen ion concentration, or pH-value, is used to determine the acidity or alkalinity of water and aqueous solutions. pH measurements can determine the strength of acids and bases as well as the direction of acid-base reactions. (1,2) In 1909, Søren Sørensen presented the idea of the pH-scale as a logarithmic way of expressing the H^+-concentration. (3) 25 years later, Arnold Beckman invented the first commercially successful electronic pH-meter. (4) Today, pH sensing is an important tool used in various industries, for instance water treatment processes and aquaculture- and food industries. (5) Many processes are pH-dependent, and determination of pH is a fundamental practice in process- and environmental monitoring as well as in studies of biological systems. (6)

The first optical fibre pH-sensor was described in 1980. (7) The combination of pH-sensing with optical fibre technology produces sensors that can be small, lightweight, resilient to electromagnetic interference and have high sensitivity. (8) Another advantage to fibre optic sensors is that they can be distributed in remote places and give continuous analytical measurements. (9) For instance, a fibre optic liquid hydrocarbon sensor could be placed in the sea near oil fields for detection of possible oil leaks. (10)

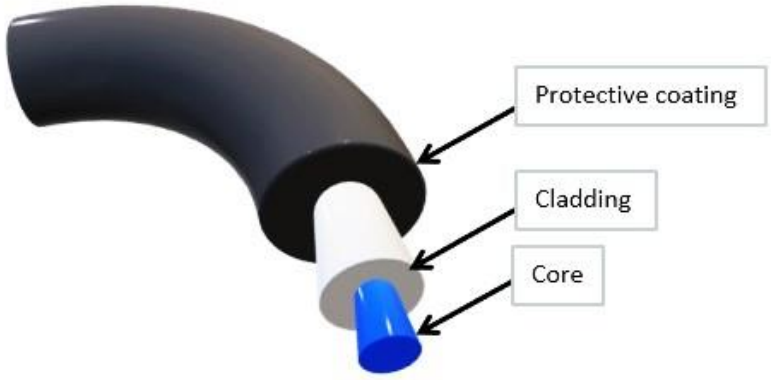

Figure 1: Schematic illustration of an optical fibre.

Chemical sensors convert chemical information (e.g. pressure, concentration, or activity of particles) into a quantifiable signal that can be analysed. (11,12) Distributed chemical sensing (DCS) is the combination of the techniques of chemical sensing and distributed fibre-optic sensing. (13) This results in a system where one can do remote surveillance of an environment with spatially resolved chemical measurements along the entire fibre. In all distributed chemical sensing (DCS) systems, there is a mechanism for converting the chemical information into some modulation of optical properties that is quantifiable. (13) The sensing mechanism can for instance be based on optical loss, bending loss, guidance loss, strain, or fluorescence emission. In this thesis, fluorescence emission and strain are the sensing mechanisms that will be explored.

Lu et al. presented in 2019 a comprehensive review of DCS methods, which included methods based on strain and fluorescence. (13) The fluorescence-based method demonstrated good selectivity and sensitivity and was showing promise for chemical analysis spanning distances of a few kilometers. In contrast, the strain based DCS method demonstrated lower sensitivity, but could be employed for longer distances, allowing chemical analysis over tens of kilometers.

The aim of this thesis is to test and apply pH-sensitive materials for interaction with optical fibres. For this, two different routes, or optical fibre sensor systems, are explored. The first pH-sensor system explored in this thesis employs a fluorescence emission DCS mechanism. The main objectives of this part of the thesis are to remove protective coating of the fibre, incorporate a fluorophore (acridine) in the cladding of the fibre, and investigate changes in optical power in air and in different pH-environments for doped- and undoped optical fibre cables.

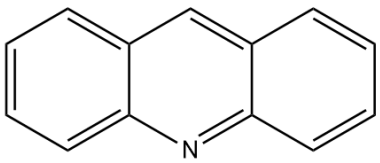

Acridine

Figure 2: Molecular structure of acridine.

A fluorophore is a molecule that can emit light upon excitation by an external energy source. (14) Acridine (Figure 2) is a fluorophore and can act as a pH indicator since the acridine's fluorescent lifetime varies with pH. (15) By doping segments of the cladding of the optical fibre cable with acridine (Figure 3), leaving gaps of suitable lengths, and measuring the fluorescent lifetime at each segment, a pH-sensitive system can be made. This thesis will document the process of making this sensor and explore some of its usability and limitations. Surveillance of the immobilization process is achieved through optical power monitoring. Comparative optical power monitor experiments, with different optical filters applied, of doped- and undoped optical fibre cables are performed in air and in Carmody buffer solutions of pH values from 4 to 9. Statistical significance of the results was assessed using analysis of variance (ANOVA), F-test, and t-test.

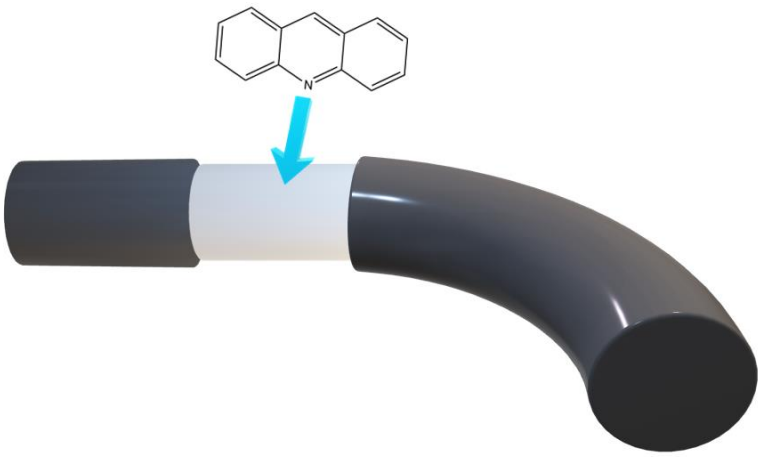

Figure 3: Acridine is immobilized in the cladding of a plastic - clad silica fibre.

The second system is based on strain-based sensing from swellable materials, thereunder hydrogels. Hydrogels are utilized in various applications where one would need environmental sensitivity. (16) While several fibre-optic pH sensors based on changes in reflection have been developed before (17–19), it remains interesting to examine and discuss the properties and useability of a selection of these stimuli responsive gels.

The main objectives of this route are to synthesize hydrogels and evaluate their ability to act as a strain-inducer in a potential strain-based optical fibre pH-sensor (Figure 4). The hydrogels are assessed based on their swelling capacities in distilled water and solutions with pH-values

ranging from 4 to 9. In a potential system, the hydrogels need to exhibit pH-dependent swelling behaviour while adhering to the optical fibre cable. Significant adherence between hydrogel and optical fibre cable is essential as the system relies on the swelling to induce detectable strain on the fibre.

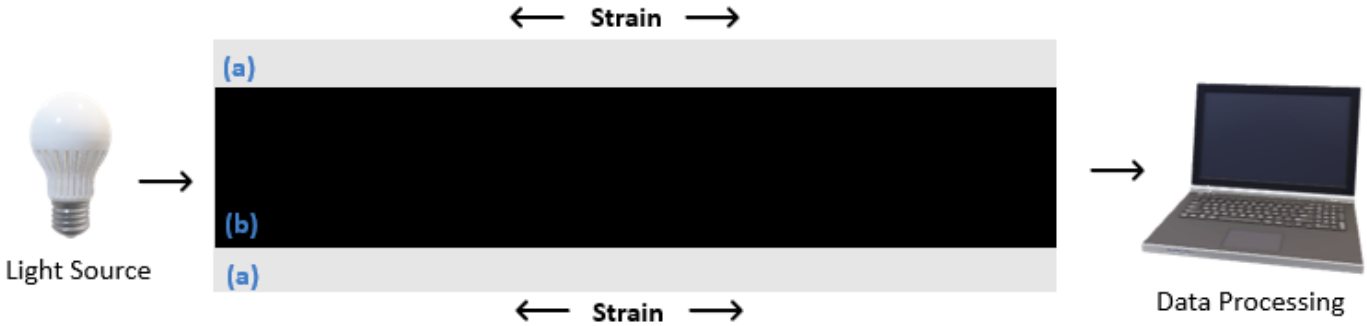

Figure 4: Schematic representation of a strain-based optical fibre sensor, where (b) is an optical fibre cable and the material that induces strain (a) is coating the fibre. (a) strains the cable through retraction and expansion in response to an analyte.

1.2 Theory

1.2.1 Previous work

Potyrailo et al. demonstrated in 1998 that intrinsic chemical sensors could be fabricated by immobilizing suitable reagents in the cladding of a plastic-clad silica (PCS) optical fibre. (20) In 2003, Scorsone et al. immobilized poly(o-methoxyaniline), an electrochromic conducting polymer, in a PCS fibre for evanescent detection of gaseous ammonia and HCl. (21) In 2019, researchers at NORCE explored the placement of a fluorophore in the core, cladding, and at the tip of an optical fibre cable, finding that the cladding was the most practical location for distributed fluorescence measurements. (13) Similarly to these articles, a sensing element is immobilized in the cladding of a PCS fibre in this thesis. However, in the present study, the element is incorporated for pH sensing.

As in this thesis, Totland et al. and Ryder et al. explored pH-sensing systems based on the fluorescence lifetime variations of acridine. (15,22) Totland et al. immobilized acridine in amine-modified silica, while Ryder et al. incorporated acridine in Nafion. In contrast to Totland et al.'s method, this thesis does not modify the silicone cladding before immobilizing the

acridine. Another difference to those pH-systems is that the sensor explored in this thesis incorporates an optical fibre, thus enabling the possibility of distributed sensing. (13) This thesis also utilizes optical power monitoring and optical filters, which are not included in the other articles.

Distributed strain-based optical fibre sensors have also been developed previously. Such as the humidity sensor of Thomas et al., where an optical fibre was coated with a hygroscopic material. (23) This strain-based sensor accurately reported the combined effects of temperature and humidity variations over a centimetre spatial scale. The optical fibre cable experienced strain as the material expanded reversibly upon water uptake. Similarly, in the present study, hydrogels are used to coat an optical fibre cable and induce strain based on swelling. However, this sensor-system is designed for pH-sensing, as opposed to humidity.

1.2.2 Fluorescence and fluorescence lifetime

Luminescence is the emission of light from any substance and ensues when an electron go from an excited state to a state of lower energy by emitting a photon. (24) Depending on the nature of the excited state, luminescence can be divided into two categories: fluorescence and phosphorescence. Phosphorescence is emission of light from triplet excited states where the electron in the excited state has the same spin orientation as the electron in ground state. (24) The return of the electron to the ground state is thus not spin allowed and the emission rate is slow. Fluorescence occurs in excited singlet states where the electron in the excited orbital is paired by opposite spin to the second electron in the ground-state orbital. The return of the excited electron to the ground state is spin allowed and occurs rapidly by emission of a photon. Fluorescence usually emits visible light, and this is emitted almost immediately after absorption of electromagnetic radiation. (25)

Merck defines fluorescence lifetime (FL) as the time a fluorophore spends in the excited state before emitting a photon and returning to the ground state. (26) A fluorophore is defined as a molecule that can emit light upon excitation by an external energy source. Depending on the fluorophore, the FL can vary from picoseconds (pico: 10^{-12}) to hundreds of nanoseconds

(nano: 10^{-9}). Phosphorescence lifetimes are approximately 10^{9} times longer than fluorescence lifetimes. (24) FL is an intrinsic property of a fluorophore and does not depend upon the method of measurement, sample thickness or fluorophore concentration. It is however affected by external factors like the presence of fluorescence quenchers, polarity, or temperature. Fluorescence quenching is a process that leads to a decrease in fluorescence intensity. (24) This can for instance be due to collision between the fluorophore and some other molecule (i.e. collisional quenching).

pH-measurements based on fluorescence lifetime have several advantages compared with the more traditional techniques that are based on fluorescent intensity. They are less susceptible to changes in excitation light intensity, photobleaching, variation in light scattering and absorption of the sample. (27)

1.2.3 An introduction to optical fibre cables

Optical fibre cables (OFC) are used to transfer information via pulses of light, which are passed through the core of the cable. (28) OFC consists of a core of high refractive index, surrounded by a cladding of slightly lower refractive index (Figure 1, p. 1). (29) One or more protective layers are typically coated over the cladding.

A light source, typically a LED diode, sends light through the core of the cable. When the core is surrounded by a cladding of lower refractive index and light is launched into the core at a sufficiently shallow angle, the light will be confined in the core by total internal reflection. (29,30) The light can travel long distances with little reduction in intensity, and can transmit information like data, voice, and images. (31) The strength of the light signal at the transmitter and receiver ends is determined by an optical power meter. (32) In fibre optics, optical power refers to the strength of the light signal transmitted through the fibre optic cable. Fibre optics are commonly applied in telecommunication services like internet, telephones, and television. (30)

Different optical fibre cables are required in the two optical fibre pH-sensor systems discussed in this thesis. Depending on the optical properties preferred, an OFC can be made from various plastics, fused silica, optical glasses, or sapphire. (29) In the acridine pH-sensor system, an OFC

with a silica core, silicone cladding and a nylon protective coating is used. This is a conventional plastic-clad silica fibre (PCS) and is typically the type of OFC used in fluorescence-based methods. (13) In the strain-based pH-sensor system a glass optical fibre is thought to be more suitable. The core would still be silica, but here the cladding would also be silica, and the protective coating could be polyimide or acrylate.

1.2.4 Introduction to hydrogels

A hydrogel refers to a three-dimensional polymer network possessing hydrophilic and viscoelastic properties, capable of absorbing and retaining significant amounts of water when in aqueous environments (Figure 5). (33,34)

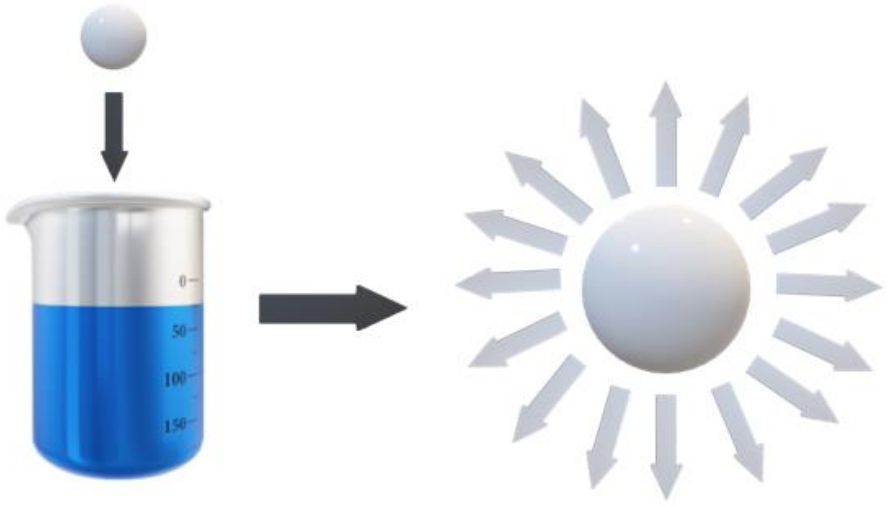

Figure 5: Hydrogels absorbs and retain water when in aqueous environments, which leads to an expansion of volume called swelling.

The properties of a hydrogel can be tailored based on the choice of monomers used in the synthesis. Stimuli-responsive polymers is a class of polymers that undergoes chemical or physical changes in response to small external changes in environment. (35) pH-responsive hydrogels can be synthesized from pH-responsive polymers that possess ionisable functional groups. Hydrogels synthesized with acidic groups will be ionised at higher pH values, and an increase in the solvent's pH will result in an increase in swelling. (16,36) For hydrogels synthesized with basic groups, lowering the pH will lead to increased swelling.

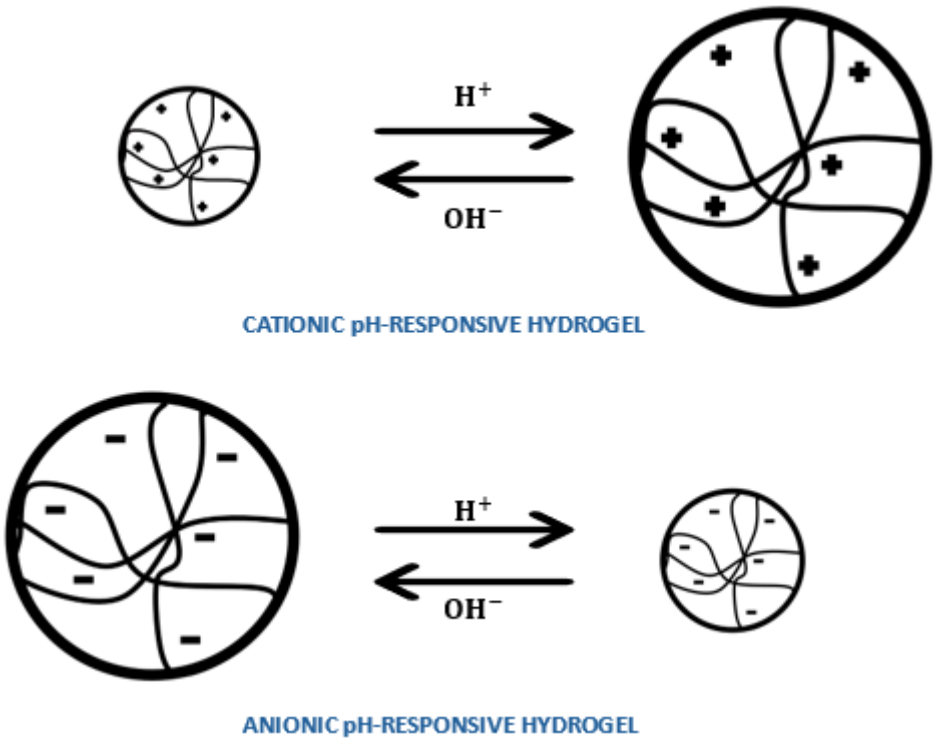

Figure 6: Schematic representation of general swelling behaviour of pH-responsive hydrogels. The cationic hydrogel swells at lower pH-values and shrinks at higher pH-values. The opposite occurs for the anionic hydrogel. Adapted from ref. (37)

Other internal factors that influence the properties of a hydrogel are the monomer-concentration, the type of crosslinker, the crosslinker density and the porosity. (37) The chemical composition, hydrophobicity and crosslinker density can for instance change a hydrogel's consistency from viscous fluid to rigid solid. (34) External factors that affect the properties of hydrogels are temperature, ionic strength, pH, and the composition of the solvent. (37) If the ionic strength of the solution a hydrogel is placed in increases, the hydrogel can exchange ions with the solution. (36) This process maintains charge neutrality and increases the concentration of free counter ions within the hydrogel. The gel swells as a result of an osmotic pressure difference that develops between the hydrogel and the solution. At high levels of ionic strength, the hydrogel will shrink due to a decreasing osmotic pressure difference between the solution and the gel. At that point, the solution will have an osmotic pressure in the range of the osmotic pressure inside the hydrogel.

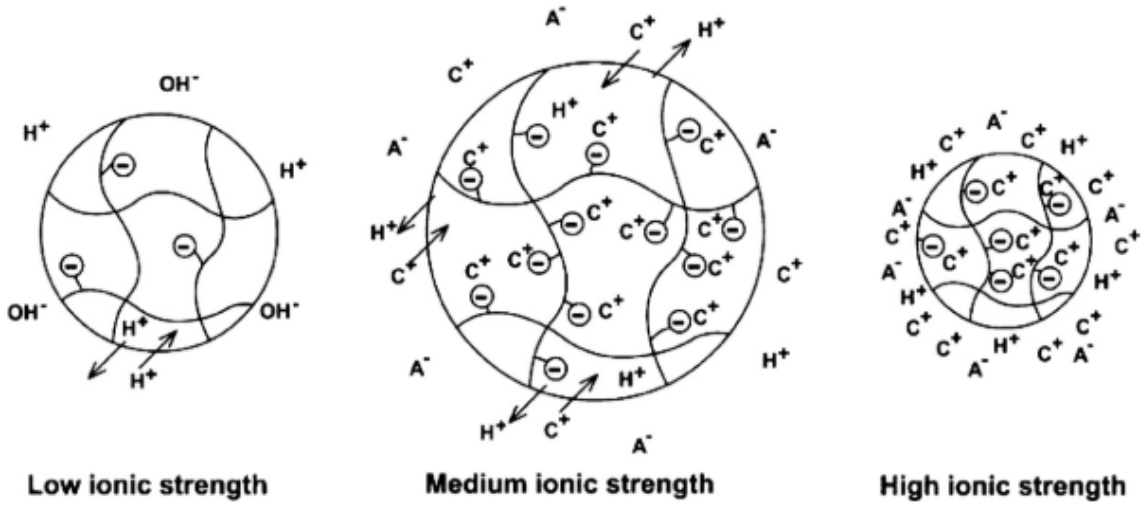

Figure 7: The effect of ionic strength on the swelling of a pH-sensitive hydrogel. Adapted from ref. (36).

1.2.5 The Carmody buffer series

The Carmody buffer solutions (38) are used in the swelling capacity experiments and in the pH-range tests of the fluorescent lifetime pH-sensor. The Carmody buffer series has several advantages compared with buffer series published earlier, which either required more chemicals, more stock solutions, standardized solutions, or covered a more limited pH range. (39–42) The preparation of the Carmody buffer series only requires two stock solutions (A and B), which are prepared from three commercially available chemicals: anhydrous boric acid (H_3BO_4), monohydrate citric acid ($C_6H_8O_7$) and trisodium phosphate dodecahydrate (Na_3PO_4).

1.2.6 Swelling capacity

The ability to swell is a characteristic property of hydrogels and is essential to investigate. (43) The degree of swelling is critical when hydrogels are applied in for instance drug delivery systems, contact lenses, or implants. (37) One common way to describe the swelling ability of a hydrogel is by measuring the swelling ratio or swelling capacity. This can be achieved through weighing, but volumetric measurements are also possible. Equation 1 is used to describe the swelling properties of the hydrogels in this thesis. The equation is adapted from the swelling

content equation described by Kipcak et al., which is based on measurements of mass variation. (43)

$$\% \, Sw = \frac{m_s - m_d}{m_d} * 100 \, \% \quad (1)$$

Here, Sw stands for swelling capacity, m_s is the mass (in grams) of the swelled hydrogel, and m_d is the mass (in grams) of the dried hydrogel. The swelling capacity is relatively calculated and quantifies the mass or volume the hydrogels gain after being immersed in distilled water or a Carmody pH-solution for a certain amount of time.

1.2.7 Free radical polymerization

In the synthesis of the hydrogels of this thesis, polymers are formed from free radical polymerization reactions. Free radical polymerization is one of the most common reactions to produce polymers. (44) The polymers are made up of vinyl monomers, i.e. monomers with the group $-\mathrm{CHCH_2}$. Free radical polymerization is a chain reaction mechanism that consists of the elementary steps of initiation, propagation, chain transfer and lastly termination. (45,46) These elementary steps are depicted in figure 8.

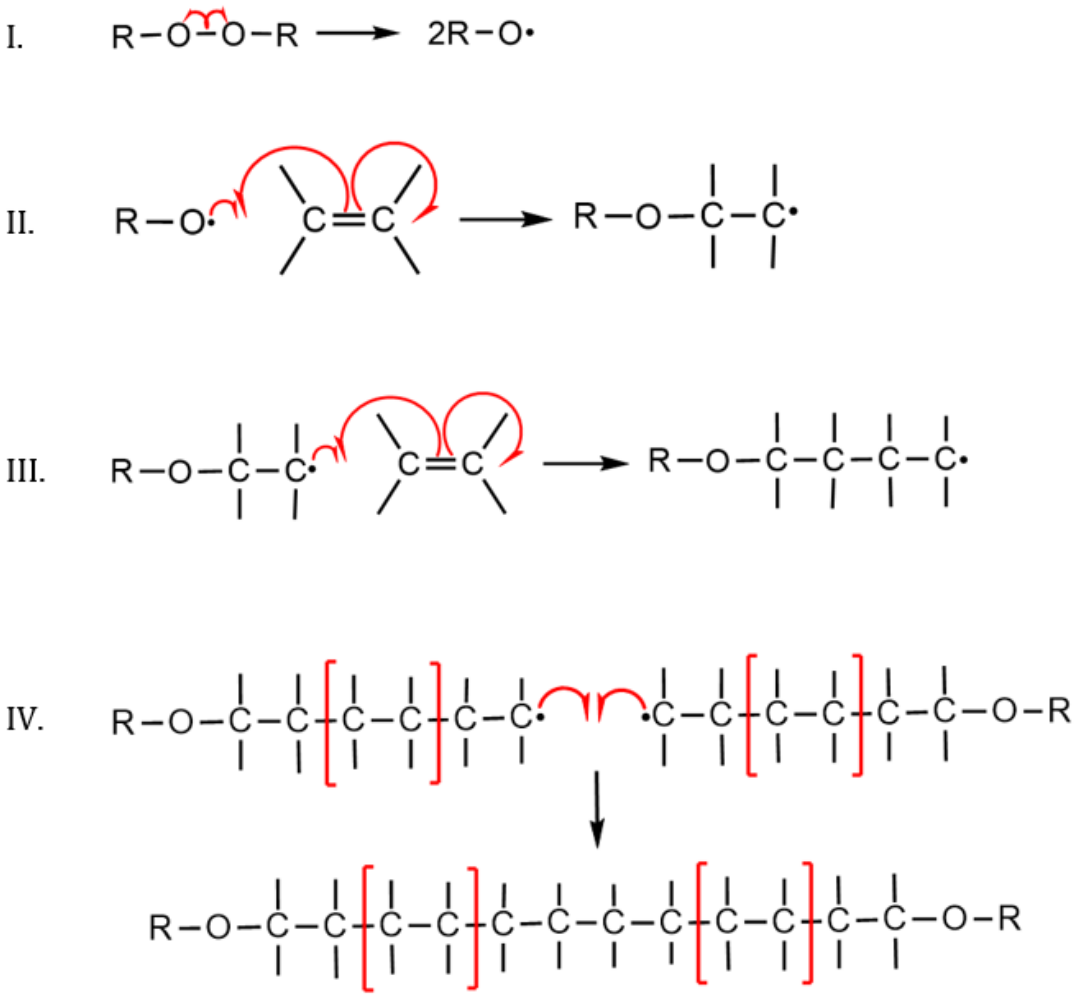

Figure 8: Steps I- IV shows the general chain-reaction mechanisms for free radical polymerization. (43) The polymerization process starts with initiator molecules that produces radicals (I). Radical molecules react with vinyl monomers and produces longer chained radical molecules (II). The chains grow longer as chained radical molecules react further with vinyl monomers (III). Termination of the chain reaction occurs when two radicals create a bond (IV).

In this thesis, acrylic acid (Aac) and N-isopropylacrylamide (NIPAM) are used as co-monomers. The molecular structures of NIPAM and Aac are shown in Figures 9 and 10.

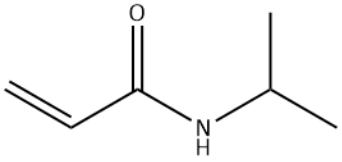

N-isopropylacrylamide

Figure 9: Molecular structure of NIPAM

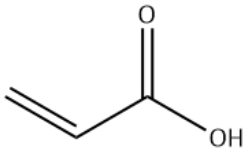

Acrylic acid

Figure 10: Molecular structure of Aac

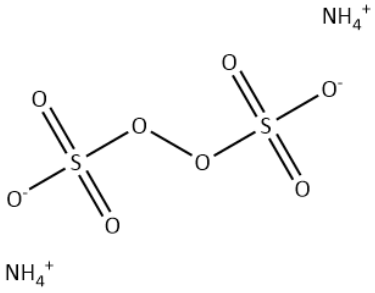

Ammonium persulfate

Figure 11: Molecular structure of APS

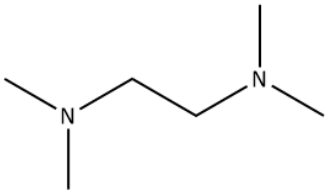

N,N,N',N'-tetramethylethyl-1,2-diamine

Figure 12: Molecular structure of TEMED

Ammonium persulfate (APS) and N,N,N′,N′-tetramethylethyl-1,2-diamine (TEMED) (Figures 11 and 12) are used as co-initiators in the gel formation reactions. APS and TEMED produces (through redox reactions) free sulphate and nitrogen-centred radicals, respectively. These radicals are highly reactive and can initiate the polymerization process. (47) The persulfate free radicals undergoes propagation reactions with the monomers, which then reacts further with monomers and thus creates polymerization chains. (48)

1.2.8 Crosslinking

Crosslinking is a process which produces network structures of polymer chains. (49) A crosslink is an ionic or covalent bond that binds two polymer chains together. If the bond between the polymers is ionic or if it is another type of weak interaction, it is called a physical crosslink. If the bond is covalent, it is a chemical crosslink. (50) Figure 13 gives an illustration to the difference in network structures of physically- and chemically crosslinked polymers. Chemically crosslinked hydrogels generally have higher mechanical strengths compared to physically crosslinked hydrogels, due to stronger bonds between the polymers. (51)

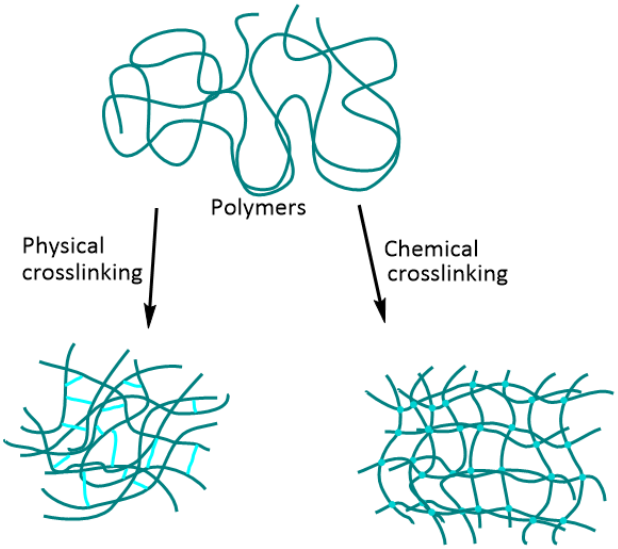

Figure 13: Schematic drawings representing physical- and chemical crosslinking of polymers. Adapted from Siqueira et al., 2023 (30).

The addition of a crosslinking agent to a liquid polymer can restrict its ability to move and thus give the polymer the characteristics of a solid or a gel. In this thesis N,N'-methylenebisacrylamide (BIS) is used as a crosslinker in the synthesis of the hydrogels. Its molecular structure is given in Figure 14. The polymer chains are crosslinked randomly by BIS, and the chemically crosslinked system, in principle, constitutes a gel.

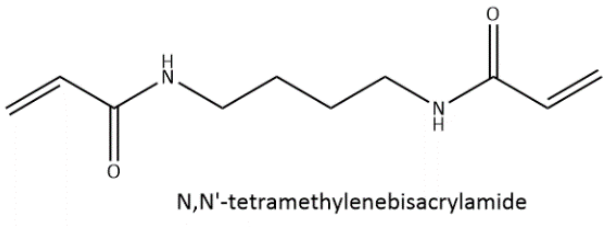

Figure 14: Molecular structure of BIS.

Crosslinking hinders dissolution of a polymer in a compatible solvent. (9) Instead, the polymer will absorb the solvent and swell to a volume where the retractive forces, that stems from stretching of the chemical bonds in the polymer, are balanced with the swelling forces that stems from the solvation of the polymer. The degree of swelling depends upon the extent of crosslinking as well as the affinity the polymer has for the solvent.

1.2.9 Degasification methods

In the preparations of the hydrogels, the solutions are degasified to remove oxygen. The removal of oxygen is important as oxygen can be a hindrance to the polymerization process, i.e. it decreases the rate of propagation by reacting with the propagating free radicals. (52) Two different methods of degasification have been employed in this thesis: ultrasonication and Schlenk line. The following subchapters a) and b) will give introductions to these methods.

a) Ultrasonication

Ultrasonic waves are soundwaves (i.e. pressure waves) that are of higher frequency than what humans can hear, with frequencies over 20 kilohertz. (53) When water is irradiated with ultrasonic waves, bubbles of certain sizes are created and undergo expansion and compression. (54) As the bubbles decrease in size the pressure within the bubble increases. Likewise, the pressure inside the bubble decreases with increasing bubble size. Differences in pressure outside and inside of the bubbles lead to diffusion of gas and/or vapour in and out of the bubbles. The diffusion tends to promote growth in bubble size rather than the opposite. Part of this effect is due to the influence of the surface area. More gas tends to be included with the bubble when the surface area is larger, than what is excluded when the surface area is smaller. This is because of the thickness of the liquid boundary increases with decreasing surface area, making it more difficult for gas molecules to travel through the boundary. When

the bubbles reach a certain size, they will collapse.(55) The generation, growth and collapse of bubbles resulting from ultrasonic irradiation is called acoustic cavitation. After the bubbles collapse, some of the gas will become fine bubbles and some will by coalescence make up larger bubbles again. Eventually, the bubbles will rise to the surface of the water due to buoyancy and thereby leave the water containing less dissolved gas than prior to the treatment. (54)

b) Schlenk line

Manifold systems with vacuum and inert gas, commonly called Schlenk lines, are used to create an air-free environment. (56,57) This is useful when reagents are sensitive to moisture, carbon dioxide or oxygen. Figure 15 shows a setup with the main components of a Schlenk line. A system of polyvinylchloride (PVC) tubes and glassware links the reaction flask to a vacuum, that removes atmospheric gas. The system of PVC tubes and glassware also connects to a supply of inert gas, typically nitrogen or argon, which fills the space previously occupied by air. The system and other equipment, like syringes, are flushed at least three times, by removing air by vacuum and exchanging it with inert gas.

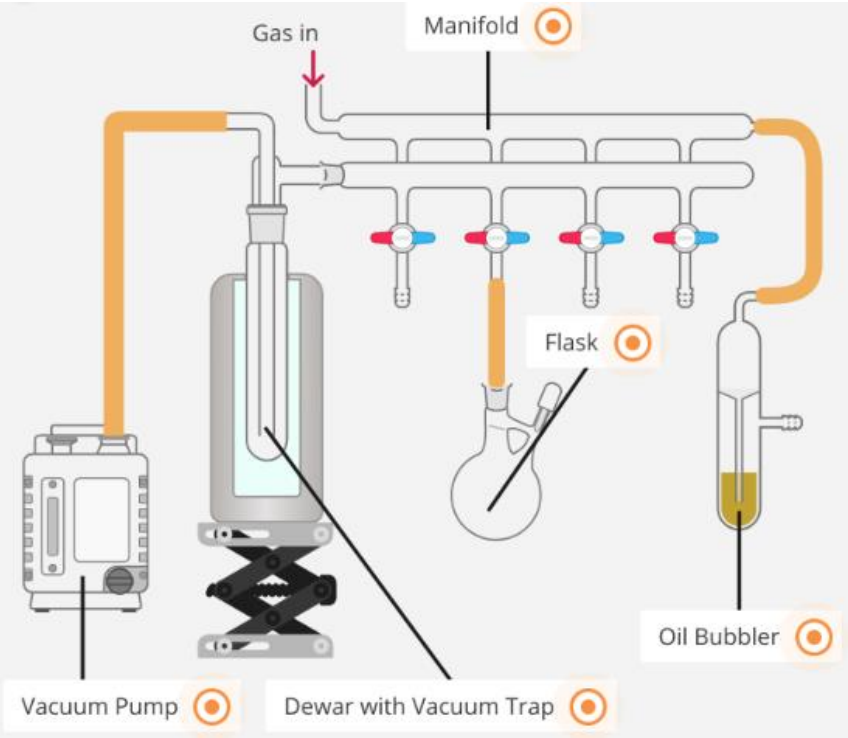

Figure 15: Schematic drawing showing the main components of a Schlenk line. (51)

2. Methods and materials

The method and materials chapter presents the equation, instruments, chemicals, and solutions alongside the methods that are used in this thesis.

2.1 Equation

Swelling capacity (37,43)

$$Sw = \frac{m_s - m_d}{m_d} \quad (1)$$

Sw stands for swelling, m_s is the mass in grams of the swelled hydrogel and m_d is the mass in grams of the dried hydrogel. The swelling capacity is relatively calculated and quantifies the mass or volume the hydrogels gain after being immersed in distilled water or a Carmody pH-solution for a certain amount of time.

2.2 Instruments

- Schlenk line
- Optical power monitor, model PM200, produced by Thorlabs.
    - In all optical power monitor experiments, a T-cube LED DRIVER (LEDD1B) and a M365L3 UV mounted 365 nm LED from Thorlabs was used. The LED DRIVER had a current of 0.4 ampere.
- pH-meter, model 6230M, produced by JENCO.
- Ultrasonic bath

2.3 Chemicals and solutions

All chemicals were supplied by Merck and used as received. The distilled water was Milli-Q type 2 water purified by an IQ 7010. All chemicals and solutions were handled in a fume hood with appropriate safety measures.

Table 1: Chemicals used in the removing-process of plastic-clad silica fibre coating.

Chemical	Molecular formula	Molecular weight [g/mol]
Propylene glycol	$C_3H_8O_2$	76.09
Acetone	C_3H_6O	58.08
Sulfuric acid	H_2SO_4	98.08

Note that in table 1, acetone and sulfuric acid were only used in preliminary experiments. After the preliminary experiments, propylene glycol was the only chemical used to remove coating.

Table 2: Chemicals used in the preparation of the acridine-dye-solution.

Chemical	Molecular formula	Molecular weight [g/mol]
Toluene	$C_6H_5CH_3$	92.14
Acridine	$C_{13}H_9N$	179.22

Table 3: Chemicals used in the synthesis of hydrogels with their abbreviation, function in the synthesis, and molecular weight.

Chemical	Abbreviation	Function	Molecular weight [g/mol]
Acrylic acid	Aac	Monomer	72.06
N-isopropylacrylamide	NIPAM	Monomer	113.16
Ammonium persulfate	APS	Initiator	228.2
N,N'-methylenebisacrylamide	BIS	Crosslinker	154.17
N,N,N',N'-tetramethylethyl-1,2-diamine	TEMED	Polymerization initiator	116.2

Table 4: Chemicals used in the preparation of the Carmody buffer stock solutions.

Chemical	Molecular formula	Molecular weight [g/mol]
Boric acid	H_3BO_3	61.84
Citric acid monohydrate	$C_6H_8O_7 \cdot H_2O$	210.14
Trisodium phosphate dodecahydrate	$Na_3PO_4 \cdot 12H_2O$	380.12

2.4 Preparation of Carmody solutions

Stock solution A contains 0.200 M H_3BO_4 and 0.050 M $C_6H_8O_7$, while stock solution B is 0.100 M Na_3PO_4. (38) The stock solutions are prepared by accurately weighing the components using an analytical balance, transferring them quantitatively into a volumetric flask, and diluting with Milli Q water.

Solutions of specific pH values are achieved by mixing the stock solutions to match pH corresponding ratios, as listed in table 5. The solutions were diluted in volumetric flasks to where the total moles (mol A + mol B) per litre of solution was equal to 0.100 M. Additionally, 3.5 weight % of sodium chloride was added to each pH solution to achieve an ionic strength comparable to common seawater. 3.5 weight % is commonly used as the average salinity of seawater. (58)

Table 5: Corresponding pH-values to stock solution ratios, where A is 0.200 M boric acid and 0.050 M citric acid, and B is 0.100 M tertiary sodium phosphate.

pH	$\frac{A}{B}$
4	3.44
5	2.03
6	1.44
7	0.98
8	0.74
9	0.53

2.5 The acridine pH-sensor system

For the acridine pH-sensor system, the following steps were taken. A method to remove the fibre coating and expose the silicone layer of the fibre was developed. An acridine dye was prepared using toluene as the solvent. Methods to impregnate the silicone layer with the acridine dye were investigated. The fluorescence lifetime and pH-dependency of the dye was explored through methods of optical power measurements.

2.5.1 Removal of the fibre's protective jacket

Propylene glycol was used to chemically remove part of the protective jacket of the optical fibre. The protective jacket was made up of nylon, and melted in a matter of minutes when the cable was submerged in boiling propylene glycol. The propylene glycol was heated in Pyrex glassware on a hotplate with temperature control. The boiling point of propylene glycol is around 187 °C. At low temperatures propylene glycol is stable in a closed container, but at higher temperatures acrid smoke and irritating fumes are emitted (59). To reduce exposure to these gases a lid was fashioned from aluminium foil. Holes were cut in the lid where the temperature measuring rod was inserted and where the fibre was to be inserted when the propylene glycol had reached its boiling point. After a segment of the fibre had been in the propylene glycol approximately five minutes it was removed and cooled in room temperature. The segment was studied to ensure that only the nylon-coating was removed, and eventual small residue of nylon was easily removed by hand.

2.5.2 Preparation of dye-solution

10 mM dye-solution was prepared by weighing in 0.8961 grams of acridine to a 500 mL volumetric flask and dissolving it with toluene.

2.5.3 Immobilization of acridine in silicone cladding

Three experiments (Im-1, Im-2 and Im-3) were conducted of the acridine-immobilizing process. The optical transmission was monitored with an optical power monitor during the soaking process. In experiment I-2 and I-3, the response of undoped cladding to soaking in tap water was tested on the optical fibre cables before they were doped.

Immobilization of the indicator dye in the silicone cladding was executed by first threading the fibre through an approximately 20 cm long nylon 6:6 tube that was slightly bent upwards in the ends, so that when it was filled with liquid, it filled up the centre of the tube (see Figure 16 for picture of the set-up). The fibre was inserted so that the part of the fibre with exposed cladding was in the middle of the tube. The dye-solution was transferred to the tube using a glass-pipette. After 20 minutes the solution was removed by piercing a small hole in the centre of the tube, and letting it drip down into a beaker glass. The cable was connected to a light source (365 nm LED) and an optical power monitor (OPM) that took one sample per second. The data was logged on a pc with Thorlabs OPM software and saved an Excel-file.

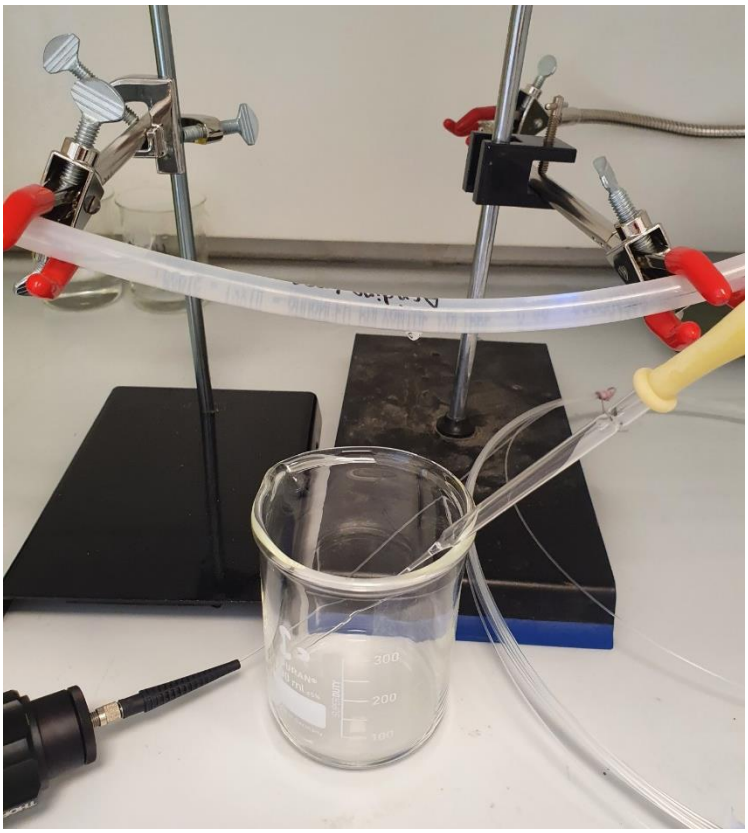

Figure 16: Picture of the acridine-immobilization set-up, before removal of remaining liquid dye. The blue light from inside the tube is fluorescent light emitted from acridine.

2.5.4 Comparative optical power monitoring experiments with acridine-doped- and undoped optical fibre cables

Three tests (Com-1, Com-2, and Com-3) were conducted to test the difference in light transmitted of an undoped plastic-clad silica (PCS) optical fibre cable (OFC) and a doped PCS OFC. In each experiment, the setup is the same for both OFCs. The effect different light filters had on the transmittance were investigated on both doped and undoped optical fibre cables. The aim of the different optical filters was to distinguish between the optical power that stemmed from the fluorescent light and the optical power that was contributed from the LED. The filters that were tested were FELH400, MF525-39 and FEL0500. Transmission data is found in the appendix, chapter A, figures A-1 to A-3. The optical fibre cable in Com-1 had one connector, while the optical fibre cable in Com-2 and Com-3 had two. The OFCs were dry and in room temperature when data was collected.

2.5.5 Optical power monitoring of acridine-doped cladding in Carmody buffer solutions

Optical power measurements with an optical power monitor were conducted to test if the fluorescence emitted from the immobilized acridine was measurable. Three experiments were conducted.

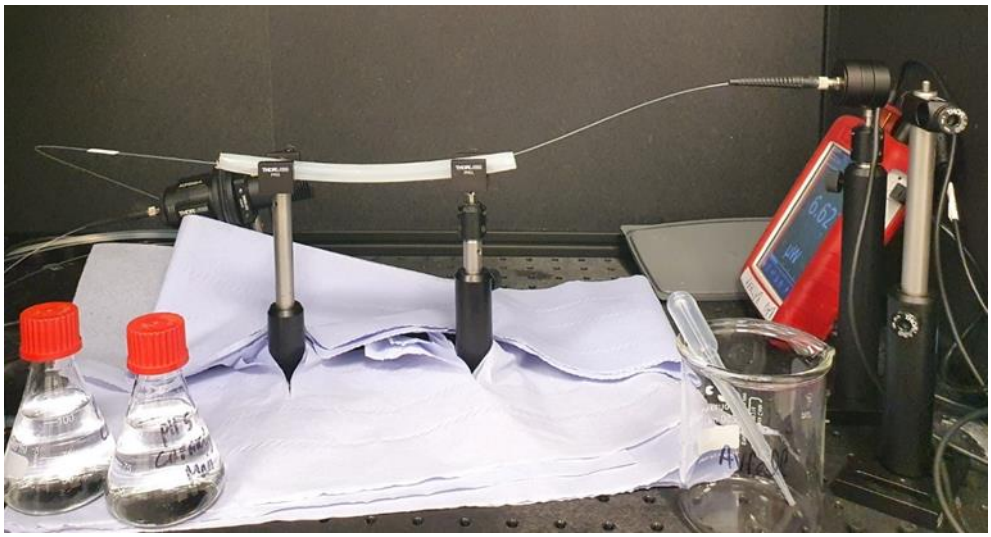

Figure 17: Setup for optical power monitor experiments with acridine-doped cladding exposed to Carmody solutions of pH-values ranging from 4 to 9.

In the first experiment (Car-1), the optical power was continuously measured while the doped cladding was exposed to air, followed by exposure of Carmody solutions of pH 4, 5, 6, 7, 8, and 9, respectively. A FELH400 filter was fitted to the set-up, see transmittance data in figure A-1 of the appendix. The optical power monitor took 1 sample per second. Cirka 2500 samples were taken with the cladding exposed to only air. Approximately 600 samples were taken in each pH-solution. When switching solutions, the tube was flushed with around 4 ml of the next solution, before completely filling the tube with the next.

In the second and third experiments (Car-2 and Car-3), Carmody solutions of pH 4, 6 and 9 were tested using two different filters. A bandpass filter (FBH470-10) was used in Car-2, and an emission filter (MF510-42) was used in Car-3. Transmission data can be found in Figures A-4 and A-5 of the appendix. The solutions and filters were selected based on the fluorescence spectra of acridine shown in Figure 18. (60) Based on the results of E. T. Ryan et al., it is expected that with the FBH470-10 filter, the optical power transmitted will be highest in the pH 6 solution. With the MF510-42 filter, the highest signal is expected in the pH 4 solution.

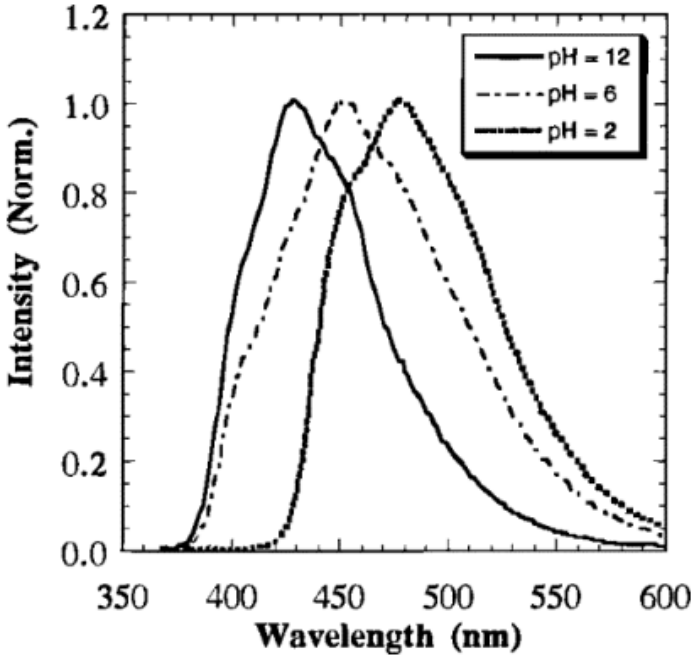

Figure 18: Fluorescence spectra of acridine in deaerated water at room temperature and pressure at three pH values: 2, 6 and 12. Normalized intensity plotted against wavelength in nanometres. Adapted from ref. (58).

2.6 The hydrogel pH-sensor system

2.6.1 Preparation of hydrogels

All hydrogels and solutions were prepared in a fume hood. Table 6 offers an overview of the main synthesis differences between the hydrogel batches.

Table 6: Overview of the main differences between the hydrogel-batches

Batch number	Total monomer concentration [M]	Ratio of crosslinker to total monomer $\left[\frac{mol}{mol}\ \%\right]$	Method of degasification	Ratio of APS to TEMED $\left[\frac{mol}{mol}\right]$
1	0.7	2.4	Ultrasonic bath and N_2 bubbling	1.9
2	0.8	2.0	Ultrasonic bath and N_2 bubbling	1.0
3	2.5	0.0048	Schlenk line	3.4
4	2	0.0060	Schlenk line	2.8
5	1.4	0.0043	Schlenk line	1.9

The polymerization was induced by free radicals with redox initiation by ammonium persulfate (APS) and N,N,N',N'-tetramethylethyl-1,2-diamine (TEMED). Acrylic acid (Aac) and N-isopropylacylamide (NIPAM) were used as co-monomers with a molar ratio of 1:1 in all five batches. In the first two batches, the total monomer concentration (concentration of AAc + concentration of NIPAM) was 0.7 M and 0.8 M, respectively. The hydrogel solutions were degased in an ultrasonic bath in the first two batches. For the following batches a Schlenk line was utilised. In batch 3-5, the total monomer concentration was 2.5 M, 2,0 M, and 1.4 M, respectively. The unit mol % is the percentage of moles relative to the total moles of monomers in the batch. In batch 1, 4.4 mol % APS was added. In batch 2, the added amount of APS was equal to 2.1 mol %. In batches 3-5, 2.27 mol % of APS was added in each. N,N'-

methylenebisacrylamide (BIS) was added as a crosslinker in all five batches. In the batch 1 and 2, 2.44 mol % and 1.95 mol % of BIS was added, respectively. In batches 3-5, the amount of BIS was reduced to approximately 0.005 mol %.

A change in crosslinker concentration is expected to affect the adhesiveness and swelling capacity of the hydrogels. Typically, materials with lower crosslink densities will exhibit higher adhesiveness to surfaces compared to materials with higher crosslink densities. (61) Decreasing the crosslink concentration may also lead to an increase in swelling capacity, as there are fewer bonds or forces present to resist expansion. (62)

Batch 1 and 2: Method with ultrasonic bath and N_2 bubbling:

Aac, NIPAM, BIS and APS were dissolved in distilled water under stirring (with a magnetic stirrer) for 30 minutes. The solution was treated in an ultrasonic bath for 10 minutes, followed by bubbling with nitrogen gas for 5 minutes. 120 µL of TEMED was added and stirred into the solution before it was transferred to 5- and 10 mL syringes, where they were left to polymerize, see Figures 19-21.

Figure 19: Picture of batch 2 taken immediately after transfer of solution to syringes.

Figure 20: Hydrogel from batch 1 after 24 hours of polymerisation.

Figure 21: Hydrogel from batch 1 removed from its syringe after 3 days.

Batch 3, 4 and 5: Method with Schlenk line:

Table 7: Stock solutions made for the synthesis of hydrogels with the Schlenk line.

Stock solution	Solute	Concentration [M]
A	Aac and NIPAM (1:1)	2.85
B	APS	1.00
C	BIS	0.012

Three stock solutions (A, B, and C) were prepared for the synthesis of hydrogels with Schlenk line (Table 7). Stock solutions were made because some of the chemicals were crystalline or solid. To avoid contaminating the system with air, the chemicals were dissolved in distilled water and transferred via syringes to the Schlenk flask through the septum. The system and all syringes were rinsed with argon gas. Stock solutions, distilled water and TEMED were all transferred via syringes to make up a total volume of 20 ml in the Schlenk flasks. Each batch used one Schlenk flask, and the solutions were stirred with magnetic stirrers. Once everything was added and stirred, with TEMED being added last, the solution was divided between two 10 ml syringes, where the solutions were left to polymerize in oxygen-free environments.

Figure 22: Picture of experiment set-up for batches 3-5, method with Schlenk line.

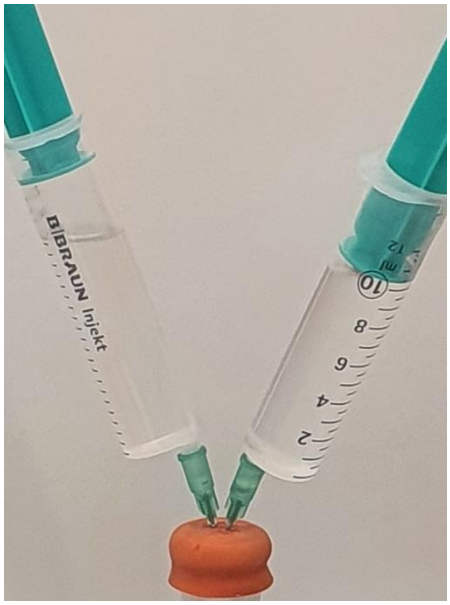

Figure 23: Samples from batch 3 immediately after the syringes were filled.

Figure 24: Same samples as in Figure 23, from batch 3, after 24 hours.

Figure 25: Sample from batch 3 immediately after removal from syringe and placed in distilled water.

Figure 26: Same sample from batch 3 as in Figure 25 after 24 hours in distilled water.

Figure 27: Sample from batch 3 after 6 months in distilled water.

2.6.2 Procedure for measure of swelling capacity

Four to five samples from batch 1 and 2 were taken to examine the hydrogels' swelling capacity in distilled water and buffer solutions ranging from pH 4 to 9. The hydrogel samples were dried at room temperature for three days and then further dried in a Termaks incubator at 50°C until constant mass was obtained. Once at a constant mass, the mass was recorded. Distilled water was then added to the hydrogels, and they were left to hydrate for one week. After complete hydration, excess water was removed, and the hydrogels were weighed again. Subsequently, the hydrogels were transferred to Carmody buffer solutions with pH values of 4, 5, 6, 7, 8, and 9, respectively. The buffer solutions were rotated every 2 days, and the mass of the hydrogels was recorded between rotations.

For samples in batch 3 and 4, a dialysis tubing method was used to examine their swelling capacities. The dialysis tubing was made up of cellulose membrane and had an average flat width of 10 mm. The tubing was cut to make 7 pieces of approximately 10 cm long tubes. The tubes were soaked in water before they were filled with samples of the gels via pipettes. Three samples were taken from batch 3 and four samples taken from batch 4. The dialysis tubes were sealed with dialysis tubing clamps, one on each end, to avoid any spillage of the samples. Similarly to the samples of batch 1 and 2, the samples were weighed after a certain amount of time spent in the different pH-buffer solutions. For these batches, the samples only rotated between pH 4, 6, 8 and 9.

3. Results and discussion

In this chapter, all results are presented and discussed in subchapters for the two routes of optical fibre pH-sensor systems that are explored in this thesis. Additionally, a subchapter of discussion regarding both sensor-systems are presented.

3.1 Results and discussion of the acridine pH-sensor System

3.1.1 The methods of removal of the optical fibre's protective jacket

One major challenge was to find a method to remove the protective coating of the optical fibre cable without inflicting damage to the underlaying layers of the cable. It became evident early in the trials that manually removing the outer coating was not a satisfactory procedure. A variety of chemical removal methods were therefore tested on a cable that was assumed to have a nylon coating. Propylene glycol was used in the first round of testing where it made no impact on the coating of the cable. Acetone was tested next, where a short piece of the cable was cut off and placed in acetone in a closed environment. This also had a limited effect on the coating. Next, a stronger polar solvent was tested, sulfuric acid. When sulfuric acid had no noticeable effect on the coating it was concluded that the protective coating could not be nylon, it was instead suspected to be Teflon. Teflon is alongside nylon a common jacket material, but Teflon is a non-polar polymer whereas nylon is polar (63). This would give an explanation as to why the methods of removal did not affect the coating.

A new cable, that was certifiably coated with nylon, was then tested with the sulfuric acid solution. It was expected that the coating would dissolve partly or wholly after 15 minutes of immersion. After only a few minutes the colour of the coating started to change and some of the coating came off the cable. If it was only nylon or also silicone that came off is uncertain, but the transmission signal changed from 610 μW to 600 μW, which, if significant, may indicate some damage to the silicone layer. This experiment proved that the coating of the two tested cables were different, and from there it was decided to go back and test with one of the gentler methods of removal. Aceton was then tested again but proved to be nonefficient with the nylon coating as well as the Teflon coating.

The propylene glycol method was then tested with the nylon-coated cable. The propylene glycol method removed the coating where the cable was immersed in the heated liquid. The cable that had its protective coating removed with sulfuric acid was more brittle than the cable that had its coating removed with propylene glycol. This indicates that more than the outer coating could have been affected when the cable was immersed in sulfuric acid. The cable also cracked and was then mechanically strengthened by attaching a thin metal rod to the cable where it was without coating to try to hinder more breakage. The optical fibre cables were examined closer with a microscope that was connected to a camera, which produced the following pictures below.

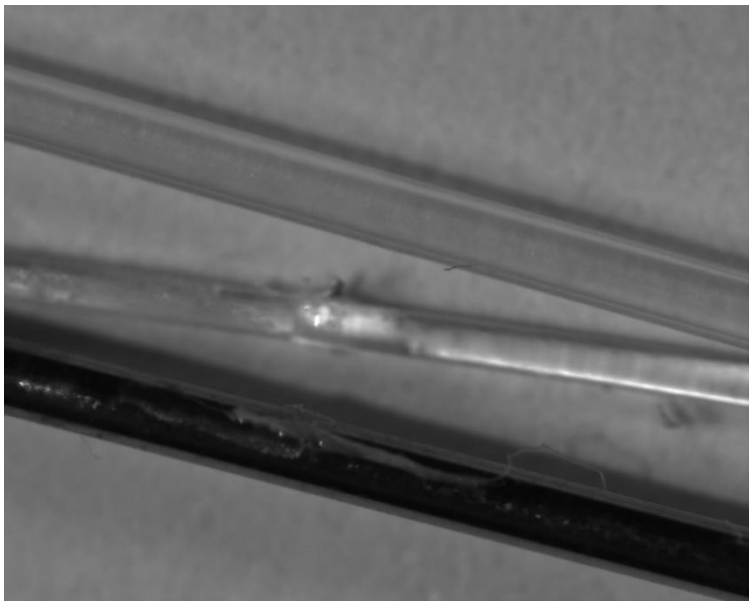

Figure 28: The cable in the middle has had its protective jacket removed with sulfuric acid. The black metal rod is used to strengthen the cable, while the other untreated optical fibre cable is included for comparison.

In Figure 28, one can see that the cable that was immersed in sulfuric acid (the cable in the middle) has an uneven surface. This indicates that the removal of the nylon layer was either not complete or that the acid removed parts of the next layer of the cable. The latter is the most likely theory as the cable was more brittle than the cable that was immersed in propylene glycol.

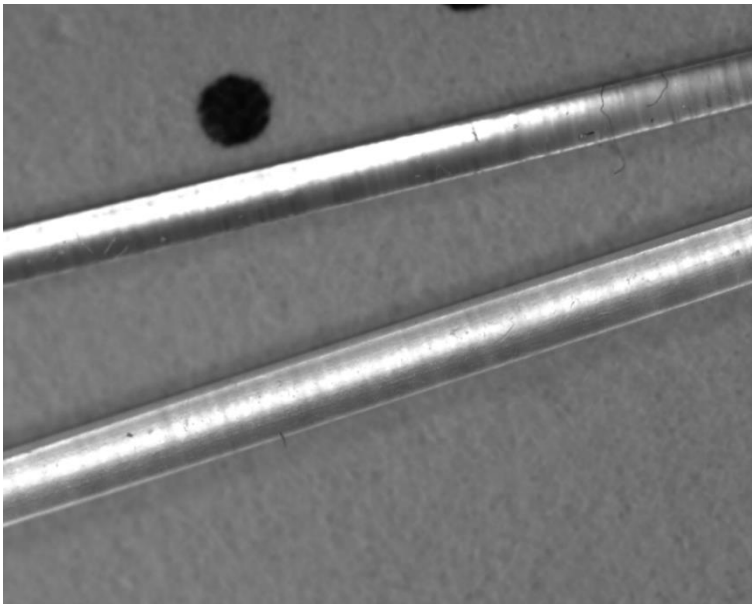

Figure 29: The uppermost cable depicted has been immersed in boiling propylene glycol. The other optical fibre cable has not but is otherwise identical.

The surfaces of the cables in Figure 29 are visibly smooth, indicating that the coating was removed evenly and likely without damaging the underlying silicone layer. Based on the condition of the optical fibre cables after undergoing their respective coating removal methods, the method using propylene glycol was determined to be preferable.

3.1.2 The immobilization of acridine in the silicone cladding of an optical fibre cable

During the soaking of the cladding in the acridine solution, blue, fluorescent light was observed, as visualized in Figure 16 (p. 20). This light was exclusively seen at the end of the coating-stripped segment where the 365 nm light first passed through. The reason the entire solution did not emit fluorescent light is likely because the acridine molecules closest to the LED source absorbed all the electron-exciting wavelengths. In a less concentrated acridine solution than 10 mM, or with a lower volume, the fluorescent light might have been more evenly dispersed due to fewer acridine molecules being present.

Dried doped claddings also emitted blue, fluorescent light when a light source was attached, although this light was of lower intensity and only visible in dark environments. The fluorescent light from the dry doped cladding was also seemingly evenly distributed, supporting the theory that lower concentrations result in more evenly dispersed fluorescent light.

The soaking time of 20 minutes was chosen based on results of Potyrailo et al. (20). They conducted real-time monitoring of an indicator-immobilization process, with their corresponding plot adapted in Figure 30. In their experiment, they found that the transmission signal stabilized within minutes of immersion of the fibre into the dye solution. The transmittance signal then remained practically constant for the following 22 hours that the fibre was immersed in the solution. 15 to 30 minutes is therefore believed to be sufficient time for acridine to be immobilized in the cladding.

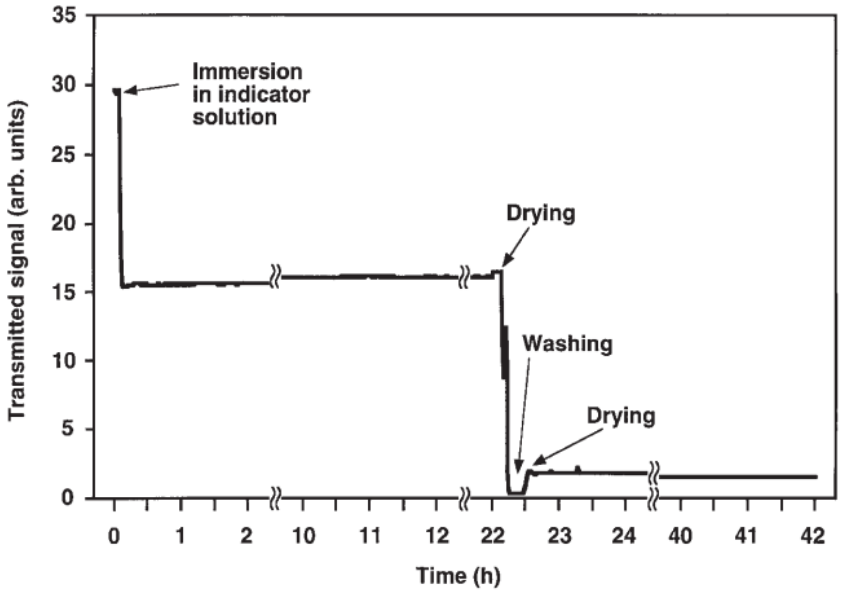

Figure 30: Plot of transmittance signal against time in hours during an immobilization process of phenol red on the silicone cladding of an optical fibre. Executed by Potyrailo et al. in 1999, ref. (48).

Table 8: Maximum signal strength and the number of connectors in each acridine-immobilization experiment.

Experiment	Maximum signal strength [µW]	Number of connectors used
Im-1	5.4	1
Im-2	1.1	1
Im-3	10.8	2

As one can see from Table 8, the max signal strength in Im-3 was significantly higher than in Im-1 and Im-2. This may be caused by the number of connectors. The cable used in Im-3 had a connector in each end. The cables used in Im-1 and Im-2 had snapped where the protective coating was removed as they were quite fragile in those segments. The low signal strengths can indicate that there was some signal loss in Im-1 and Im-2. Parts of the light may not have reached the detector when there was no connector to assure a correct and stable position of the cable end. Different setups can also contribute to variations in maximum signal strength. Attachments like extenders and focus-lenses can alter the distance the light is travelling and can redirect the light. To get more comparable results, a doped and an undoped optical fibre is tested under the same conditions in the next subchapter.

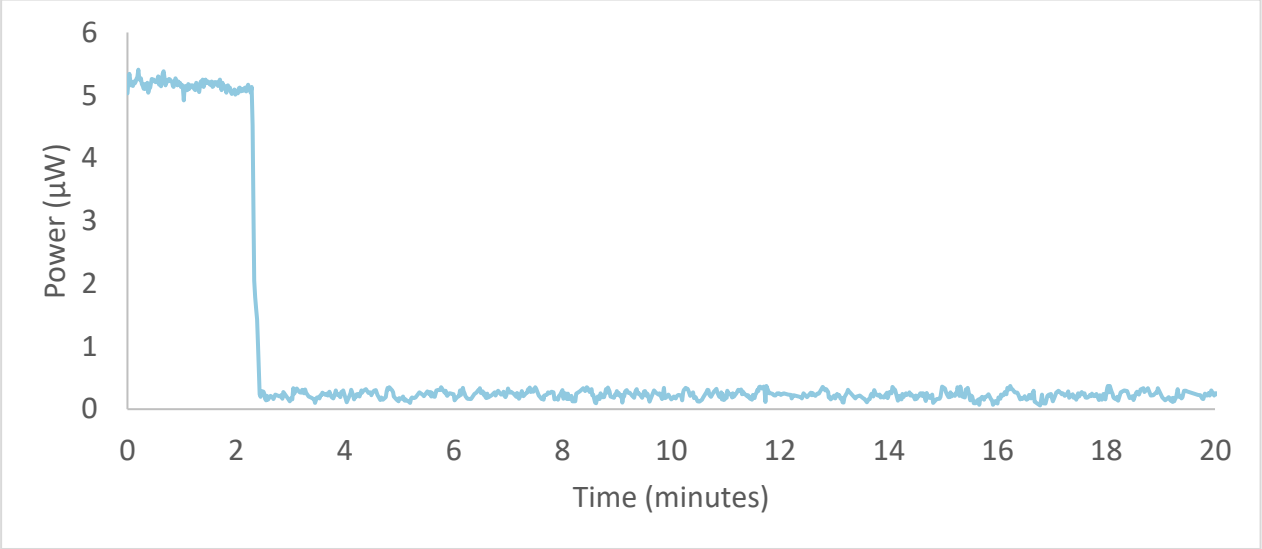

Figure 31: Im-1, surveillance of the acridine immobilization process by optical power monitoring. Power in watts is plotted against time in minutes. There is an immediate drop in signal at approximately 2.2 minutes due to the immersion of cladding in the dye.

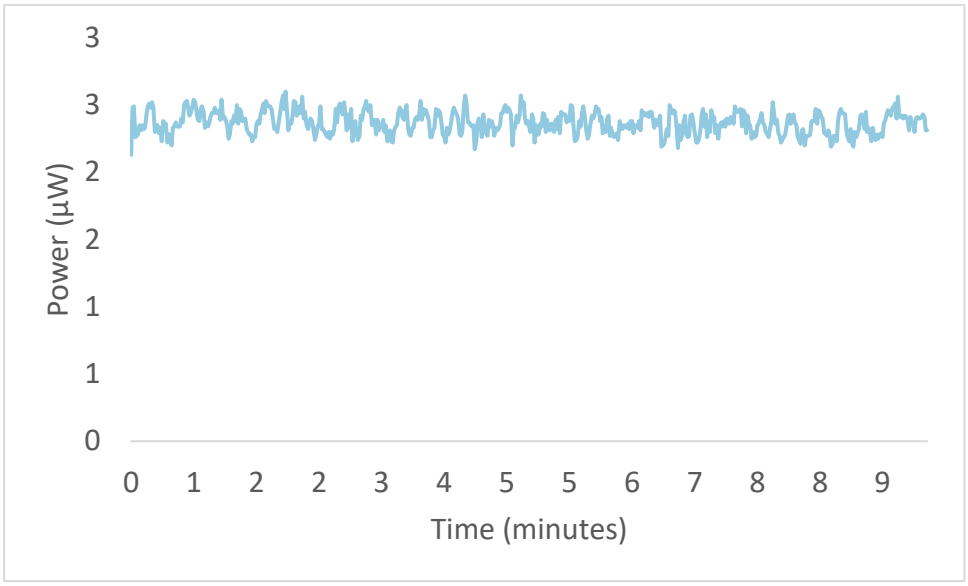

Figure 32: Response-test of undoped cable (used in Im-2) to tap water. Power in microwatts plotted against time in minutes.

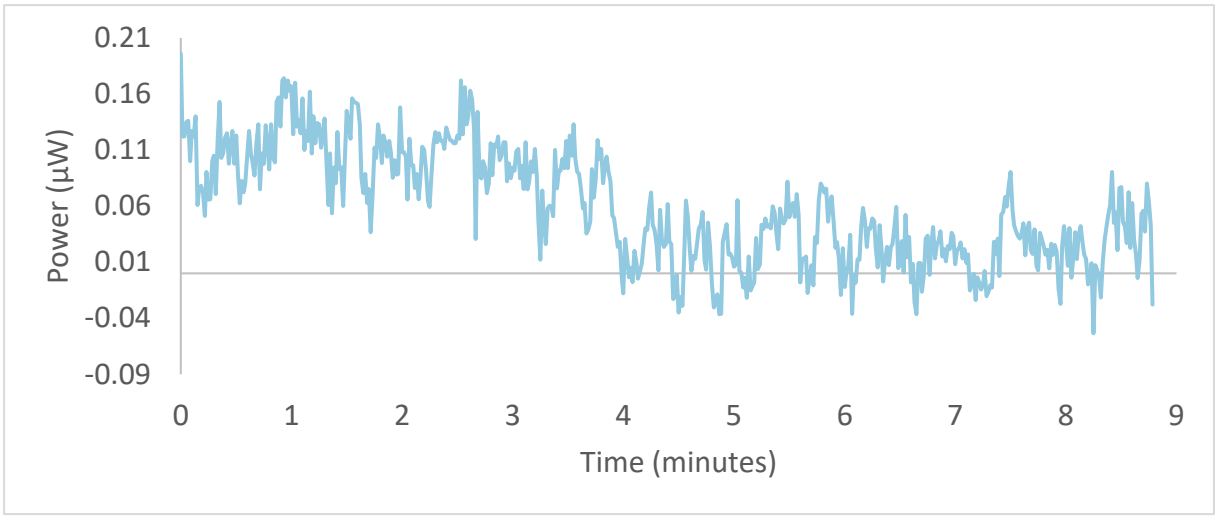

Figure 33: Im-2, surveillance of the acridine immobilization process by optical power monitoring. Power in watts is plotted against time in minutes. The drop in signal after 4 minutes is due to the cladding's exposure to the dye.

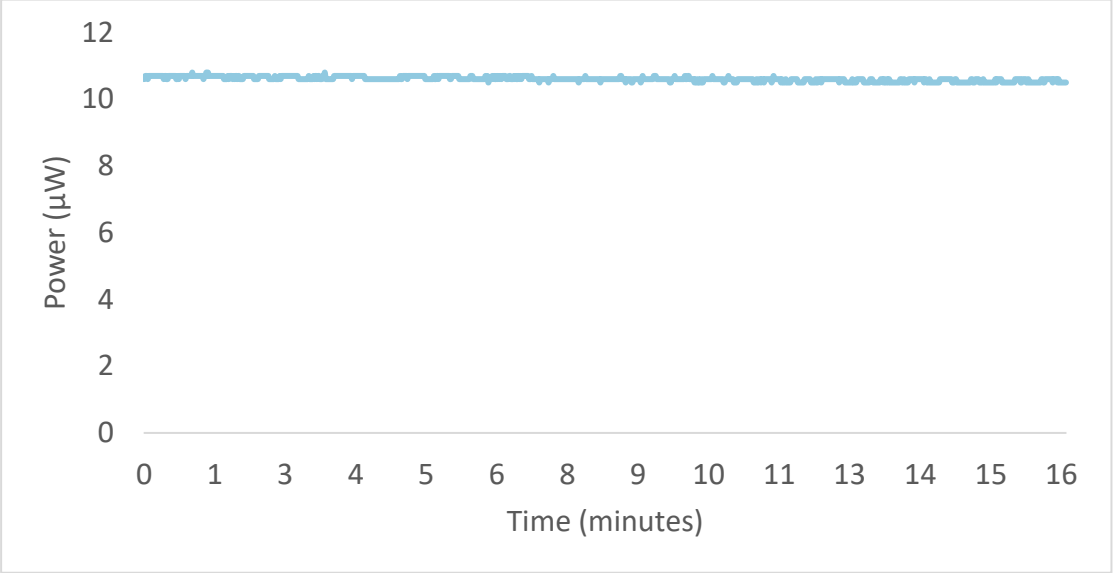

Figure 34: Response-test of undoped optical fibre cladding to tap water. The same cable is used in Im-3. Optical power measured in watts against time transpired in minutes.

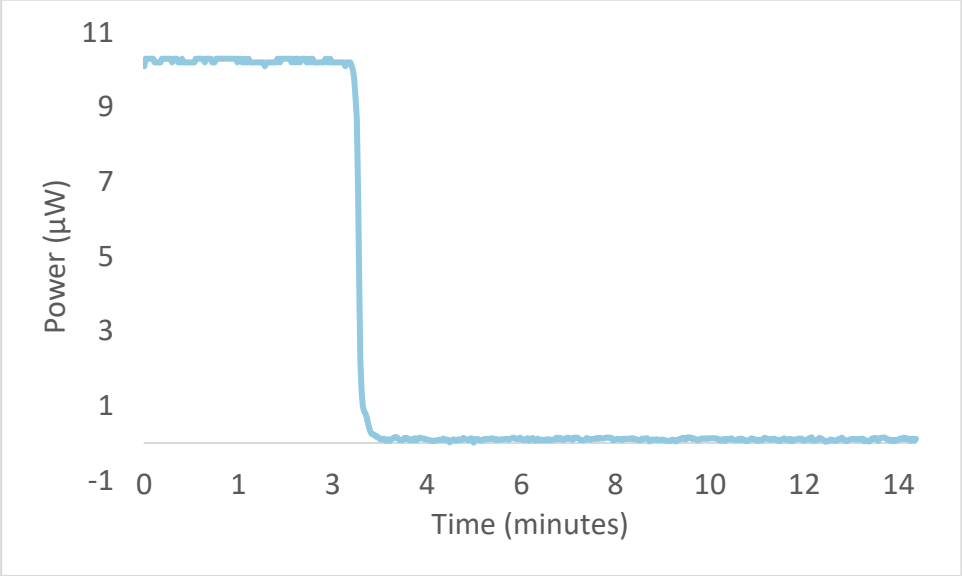

Figure 35: Im-3, surveillance of the acridine immobilization process by optical power monitoring. Power in watts is plotted against time in minutes. There is an immediate drop in signal at approximately 3.3 minutes due to the immersion of cladding in the dye.

The response-tests of undoped optical fibre cladding to water were executed to assure that it was not the cladding's immersion into a liquid that caused the drop of transmission in experiment Im-1. As one can observe from the plots in Figures 32 and 34, tap water did not have any measurable effect on the optical power signal. There was no drop in signal when the

cladding came in contact with water. As observable in Figures 31, 33 and 35, the optical power transmitted drops in all three experiments when the acridine solution came in contact with the cladding. This suggests that it was not the act of immersion into a liquid that caused to affect the signal, it was the acridine molecules that was the cause of the drop in transmittance.

The signal strength in Im-2 was too low, with a maximum of 1.1 µW. Compared to the equivalent plots of Im-1 and Im-3, shown in Figures 31 and 35, respectively, the graph in Figure 33 is highly undefined. In Im-2, there is a slight drop in signal at approximately 4 minutes. In contrast, the effect of the acridine solution on optical power is clearly demonstrated in the Im-1 and Im-3 experiments, where the graphs show a significant and momentary drop in signal when the cladding is exposed to the dye. These signal drops in Im-1 and Im-3 align with expectations based on previous results by Potyrailo et al. (Figure 30). These results indicate that a few minutes of immersion are likely enough to immobilize the acridine in the cladding. However, as shown in Figures 31 and 35, the signal remains stable after a few minutes of immersion, and longer immersion times do not negatively affect transmittance. To avoid any potential issues from too short an exposure, the fibres were immersed for 15 to 30 minutes, even though a couple of minutes would probably suffice.

3.1.3 Comparative optical power monitor experiments with doped and undoped plastic clad-silica optical fibre cables in air

The comparative experiments with doped and undoped optical fibres were conducted to investigate the effect of the acridine-doped cladding. Different light filters were tested with the aim of distinguishing between the optical power that stemmed from the fluorescence and the LED.

Ryder et al. investigated the fluorescence behavior of acridine as a function of pH in aqueous phosphate buffer and incorporated in Nafion. (22) They found that there was very little difference in the absorption spectra of acridine in solution and acridine in Nafion, with both having absorption maxima at 354.5 nm (Figure 36). They concluded that the weak absorbance of the neutral and protonated acridine species over the 370 to 390 nm range was still sufficient for reasonable excitation efficiency using a 380 nm LED. In the present study, a 365 nm LED is

used as the light source. Figure 37 shows the wavelength spectrum of the light emitted by the diode. Based on their findings, it is assumed that the range of the 365 nm LED is also sufficient for reasonable excitation efficiency.

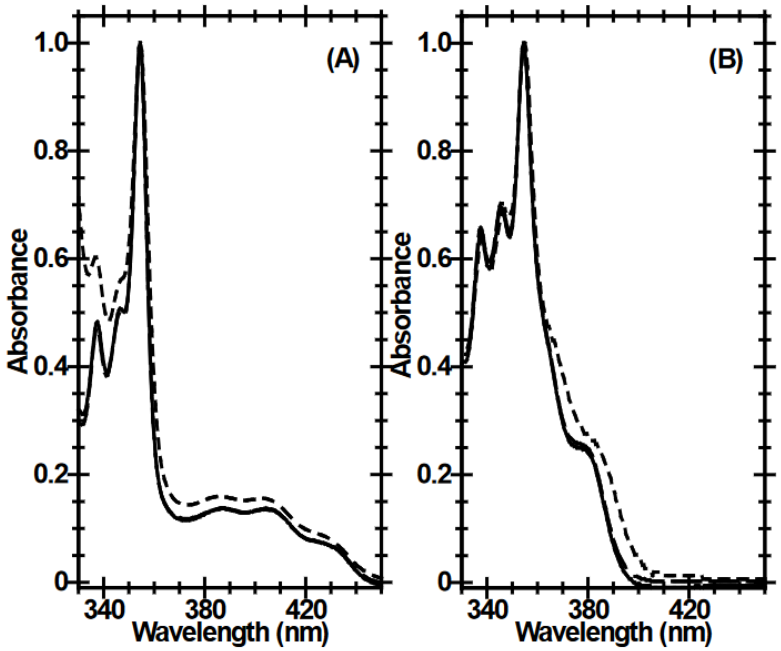

Figure 36: Absorption spectra of 0.05 mM acridine (Ac) in solution (- - -) and immobilized in purified (— —) and unpurified (—) Nafion recorded in (A) 1 M HNO_3, showing the protonated AcH^+absorption, and in (B) 1 M $NaOH$, showing the neutral Ac absorption. The spectra were normalized at absorption wavelength 354.5 nm. The figure is adapted from ref. (21)

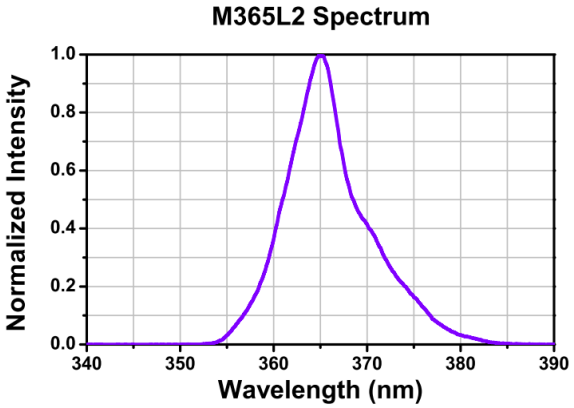

Figure 37: Wavelength spectrum of the 365 nm LED diode used in the acridine immobilisation process and in subsequent experiments. (63) The x-axis in the plot is wavelength in nanometres and the y-axis is normalized intensity.

The steady-state fluorescence emission spectra (Figure 38) show that the AcH^{+*} (asterisk denotes excited state) in solution and acridine-doped Nafion in acid have fluorescence maxima at 475 nm and 473 nm, respectively. (22) The neutral Ac^{*} species in solution fluoresces at a shorter wavelength with a maximum at 430 nm. Based on these results, broadband emission is expected from 400 nm and up in this thesis. The emission maximum depends on the environment of the acridine and is therefore difficult to predict.

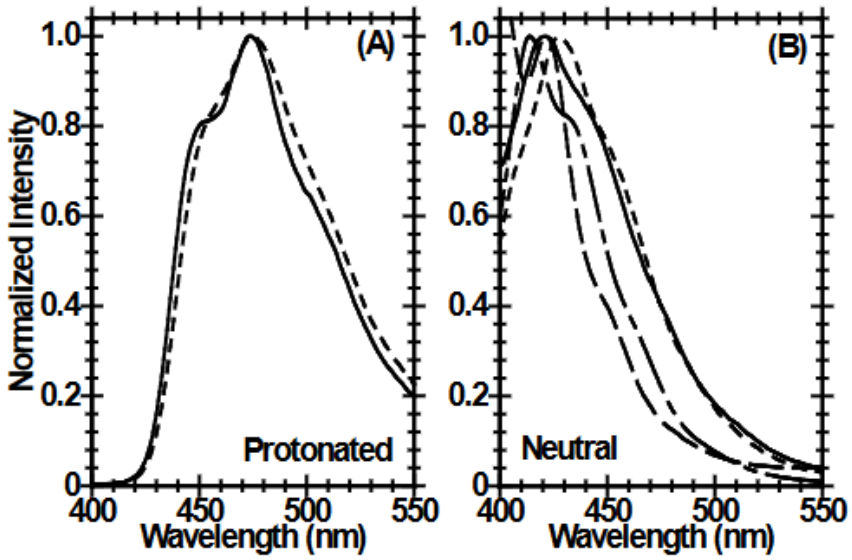

Figure 38: Normalized fluorescence emission spectra recorded in (A) 1 M HNO_3 of acridine in solution (- - -) and immobilized in Nafion (—), and (B) in 1 M $NaOH$ of acridine in solution (- - -), acridine immobilized in Nafion in 1 M $NaOH$ (—), acetone (— —) and ethanol (— - —). The figure is adapted from ref. (21)

Table 9: Average transmitted optical power in µW and ratio of transmitted power of doped and undoped optical fibre cables (OFCs) with and without optical filters

	Average optical power [µW]	Ratio (doped to undoped)
Doped OFC without optical filter	768	0.46
Undoped OFC without optical filter	1672	
Doped OFC with FELH0500 filter	0.299	1.17
Undoped OFC with FELH0500 filter	0.257	
Doped OFC with FELH400 filter	5.28	0.67
Undoped OFC with FELH400 filter	7.95	
Doped OFC with MF525-39 filter	0.088	1.23
Undoped OFC with MF525-39 filter	0.073	

The average optical power values listed in Table 9 are calculated from the minimum and maximum values listed in Table B-1, found in Chapter B of the appendix. The transmission data for the optical filters FELH400, MF525-39, and FELH500 are found in Chapter A of the appendix. The ratio of doped to undoped transmitted signal was highest when the FELH500 and MF525-39 filters were applied, with ratios of 1.17 and 1.23, respectively. With the FELH500 and MF525-39 filters, very little light from the diode reaches the detector. This results in a larger proportion of the optical power signal originating from fluorescence compared to the other filters.

Without a filter and with the FELH400 filter, the optical power in the doped fibres is reduced by approximately half and a third, respectively. This reduction may be because most of the optical power signal stems from the LED, even with the FELH400 filter. When the fibre is doped, part of the light is absorbed by acridine. The amount of fluorescent light reaching the detector is likely small, as the fluorescent light travels in all directions and is not redirected or reflected into the cable like the light from the diode. Thus, in these cases, the transmitted light is reduced when the cable is doped.

Figures 39 to 43 are based on the minimum and maximum values found in Table B-1. The effect the optical filters had on transmitted optical power relative to no optical filter is illustrated in Figure 39.

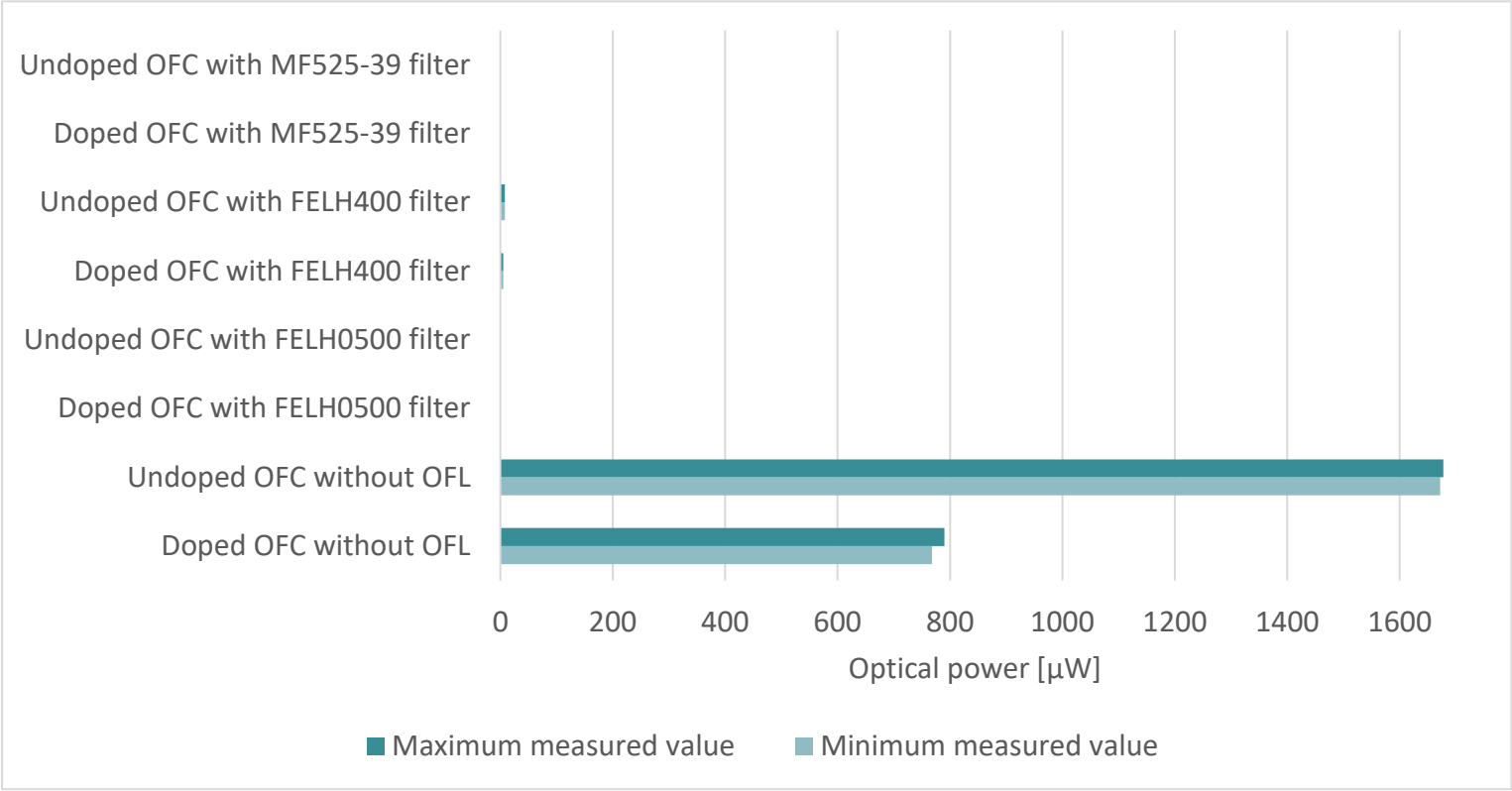

Figure 39: The diagram is based on the data in Table 9. The x-axis is optical power in microwatts. The darker colour represents the maximum value while the lighter colour represents the minimum value.

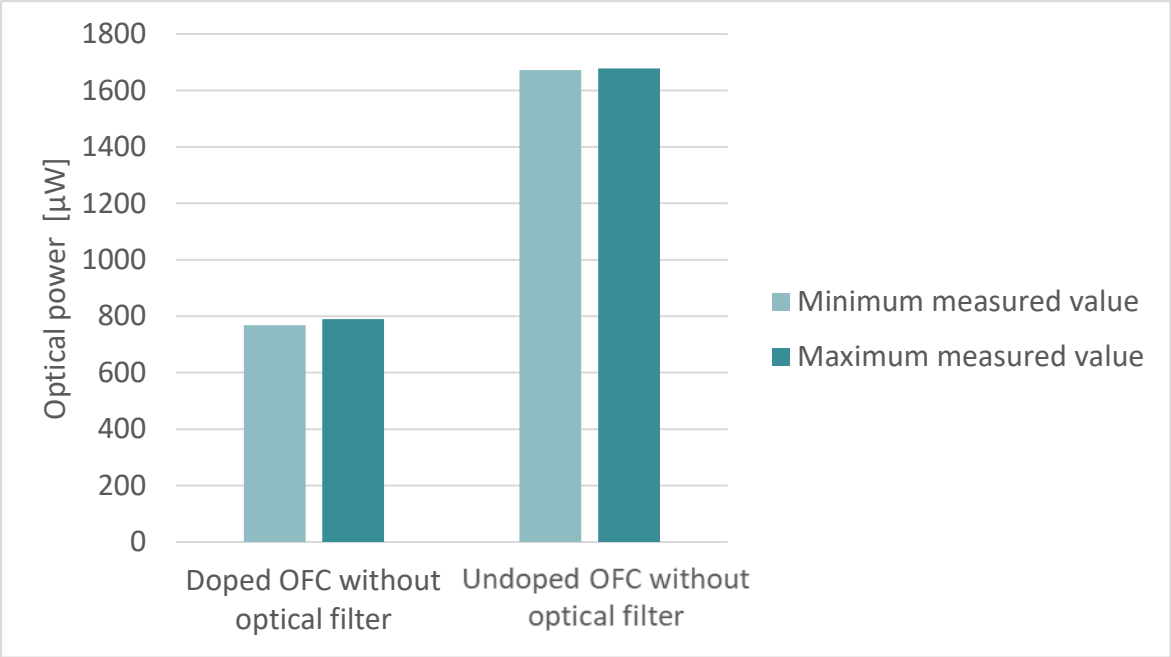

Figure 40: Optical power in microwatt measured on doped and undoped optical fibre, without optical filters applied.

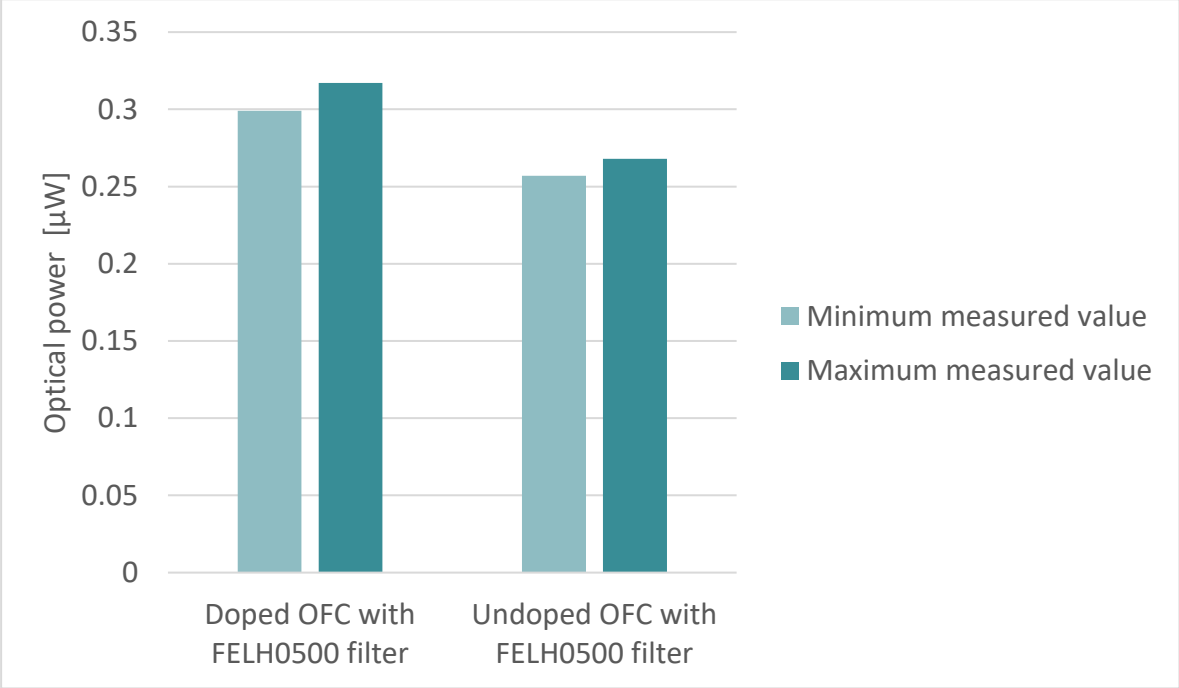

Figure 41: Optical power in microwatt measured on doped and undoped optical fibre, with FELH0500 optical filter applied.

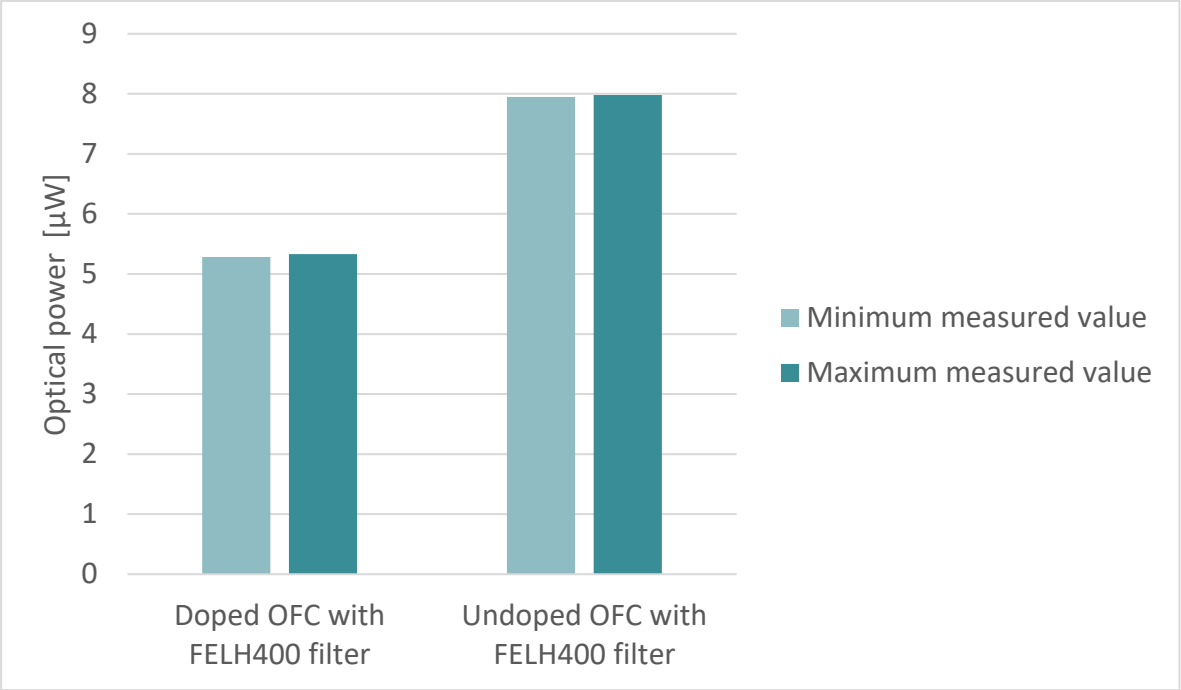

Figure 42: Optical power in microwatt measured on doped and undoped optical fibre, with FELH400 optical filter applied.

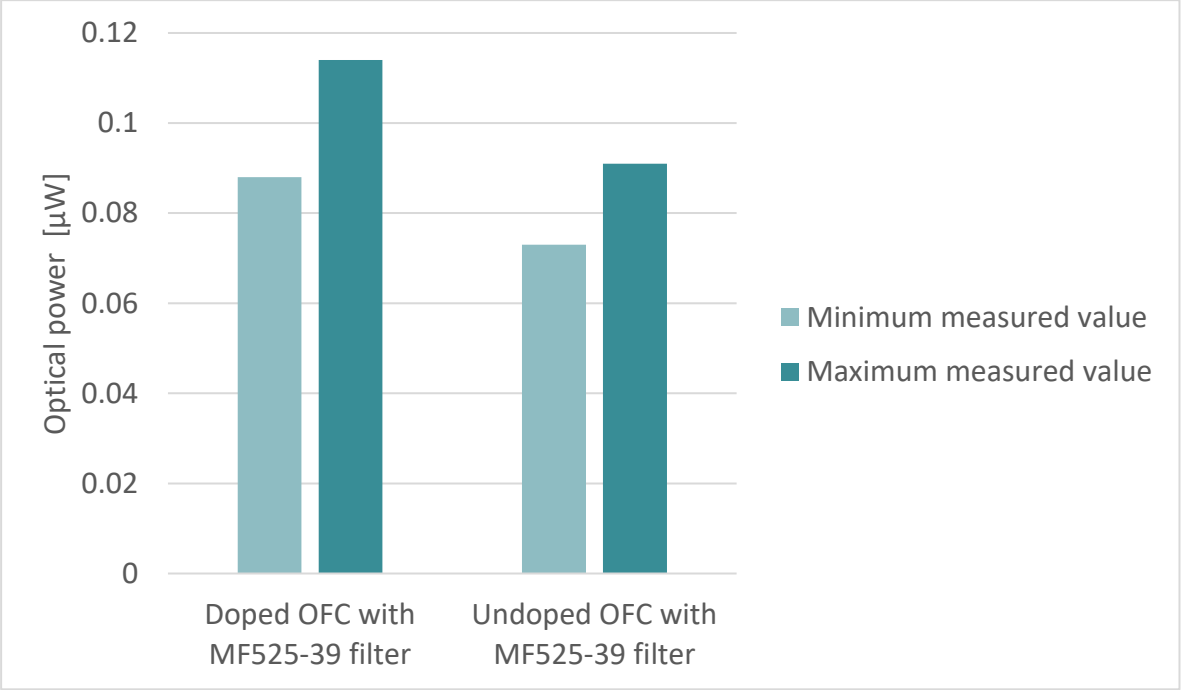

Figure 43: Optical power in microwatt measured on doped and undoped optical fibre, with MF525-39 optical filter applied.

3.1.4 Optical power monitoring of acridine-doped optical fibre in Carmody buffer solutions

An optical power monitor was used to study the response of an acridine-doped cable to different pH-environments. Initially, there was an issue with the optical power signal not stabilizing. 20-minute, 1-2 hour and 15–16-hour tests were conducted where all tests had mean signals that increased over time, when a flat graph was to be expected. By decreasing the power of the LED driver, the issue was resolved.

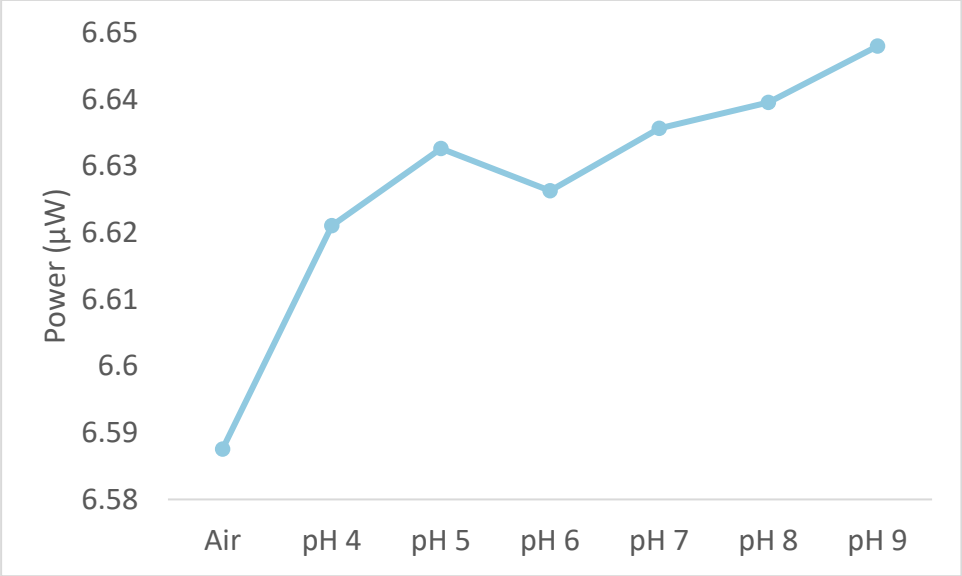

Figure 44: Car-1, plot of average optical power signal while cladding is in air and Carmody solutions ranging from pH 4 to 9.

The average optical power signal when the cladding is exposed to air and the Carmody solutions from pH 4 to 9, in experiment Car-1, is plotted in Figure 44. Statistical tests found that at a 5 % significance level, the average optical power signal in air was significantly lower than the signals detected in the Carmody solutions. Additionally, the average optical power in the pH 5-solution was significantly higher than the average signal in the pH 4-solution. From pH 5 to 6, 6 to 7, 7 to 8 and 8 to 9, the average signals were not found to be significantly different. However, the average signal in pH 4 was significantly lower than the average signals in pH 7, 8 and 9. Also, the average signals in pH 5 and pH 7 were significantly lower than the average signal in pH 9. And the average signal in pH 6 was significantly lower than in pH 8 and

9. These results indicate that optical power monitoring of an acridine-doped optical fibre could produce a low-selectivity pH-sensor. However, fluorescence lifetime monitoring is a better option as it would produce a sensor with far better selectivity and sensitivity. (13) The statistical data are found in chapter E of the appendix.

The FELH400 filter that is applied in experiment Car-1 has a cut-on wavelength at 400 nm. The transmission data of the filter is shown in Figure A-1 of chapter A of the appendix. Based on the wavelength spectrum of the LED (Fig. 37, p. 36), very little light from the light source will reach the detector when this filter is applied. Therefore, the optical power signal is expected to consist mostly of fluorescent light, which generally has longer wavelengths than the light from the LED. Since fluorescent light is emitted in all directions, only a fraction of it reaches the detector. If all the fluorescent light could reach the detector, more of the average signals might have been significantly different.

The plots in Figures 45 and 46 are based on the average optical power transmitted in Carmody solutions of pH 4, 6 and 9. Figure 45 shows the results of the experiment with the FBH470-10 filter, and Figure 46 shows the results with the MF510-42 filter.

In Car-2 it was expected that with the FBH470-10 filter there would be a higher average optical power signal when the cladding was in the Carmody solution of pH 6 and 4 than in the solution of pH 9, based on the acridine fluorescence spectra of Ryan et al. (60) (Figure 18, p. 22). In the fluorescence spectra, pH-environments of 2, 6 and 12 resulted in intensity peaks at approximately 480, 450 and 430 nm, respectively. The FBH470-10 filter has a central wavelength at 470 nm and full width at half maximum of 10 nm (Figure A-4), which overlaps best with the peaks at 480 and 450 nm. The expectations correspond with the trend of the average values shown in Figure 45. However, analysis of variance found that on a 5 % significance level, the average power values were not significantly different. This result was unexpected based on the results of the statistical tests in Car-1.

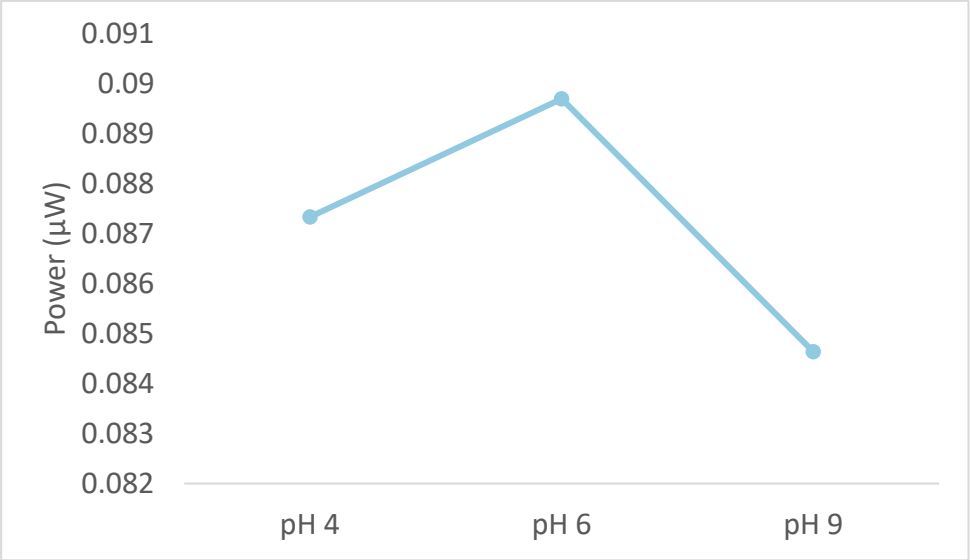

Figure 45: Car-2, Optical power monitoring in Carmody solutions of pH 4, 6 and 9 with a FBH470-10 optical filter applied.

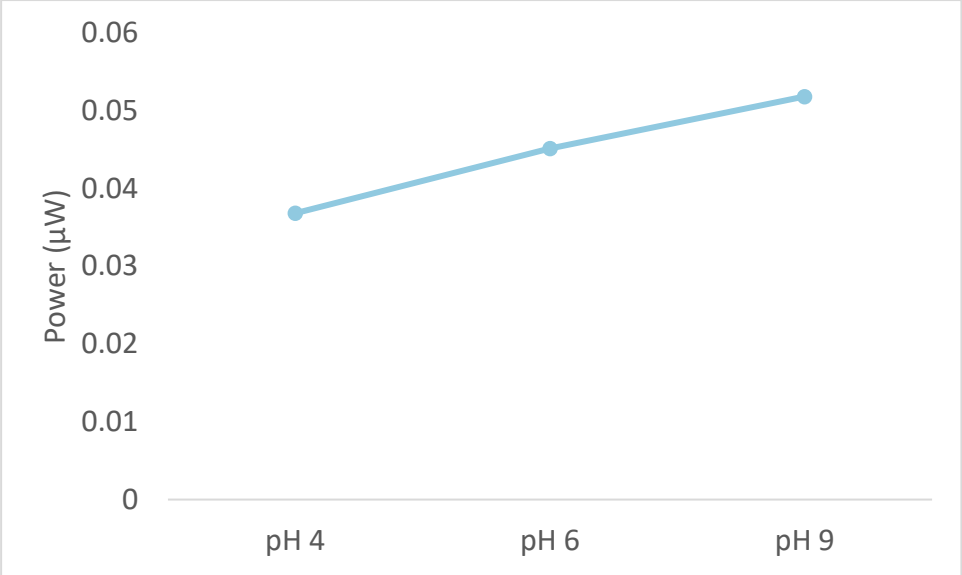

Figure 46: Car-3, Optical power monitoring in Carmody solutions of pH 4, 6 and 9 with a MF510-42 optical filter applied.

With the MF510-42 filter applied, it was expected that the highest optical power signal would be obtained when the cladding was in the pH 4 solution compared to the signals in pH 6 and 9 solutions. Contrary to this expectation, Figure 46 shows that the lowest optical power signal was obtained in the pH 4 solution. Statistical tests found that, at a 5% significance level, the average signal in pH 9 is significantly higher than the average signal in pH 4. The average signal

in pH 6 was not significantly different from the average signals in pH 4 and pH 9. This unexpected result may indicate that the fluorescence intensity peaks in this study do not match those in the study by Ryan et al. (60), possibly due to differences in the environment of the fluorophore.

3.2 Results and discussion of the hydrogel pH-sensor system

3.2.1 The swelling capacity of the hydrogels

Initially, it was planned to swipe off excess water from the swollen hydrogels with paper tissues before weighing them. However, because of the deformation and fragmentation that occurred from the drying process it was thought to be best to keep them in their containers, and carefully remove excess water by decanting and drying for short periods in a Termaks incubator to avoid loss of sample.

Table 10: Swelling capacities of samples from batch 1 and 2.

Sample number	Batch	Sample taken from hydrogel nr.	Swelling capacity [g/g]
1	1	1	155
2		1	159
3		1	173
4		2	287
5		2	146
6	2	1	60
7		2	66
8		2	126
9		3	79
10		3	82

In the swelling capacity experiments of batch 1 and 2, all hydrogels were split to make two or three samples. The only exception is sample 6 which was a small, undivided hydrogel. The shape of the hydrogel and the size of its surface area may have a significant effect on the swelling capacity of the gel. This hypothesis is based on observations, as measurements of the hydrogels' surface areas has not been made. From Table 10 one can see that sample 6 had the smallest swelling capacity. The splitting of the hydrogels resulted in rougher surfaces and some rifts and breakage of their structures. Sample 6 is the only sample that consists of an

undivided hydrogel, and it was therefore expected that it would have the smallest surface area relative to its size.

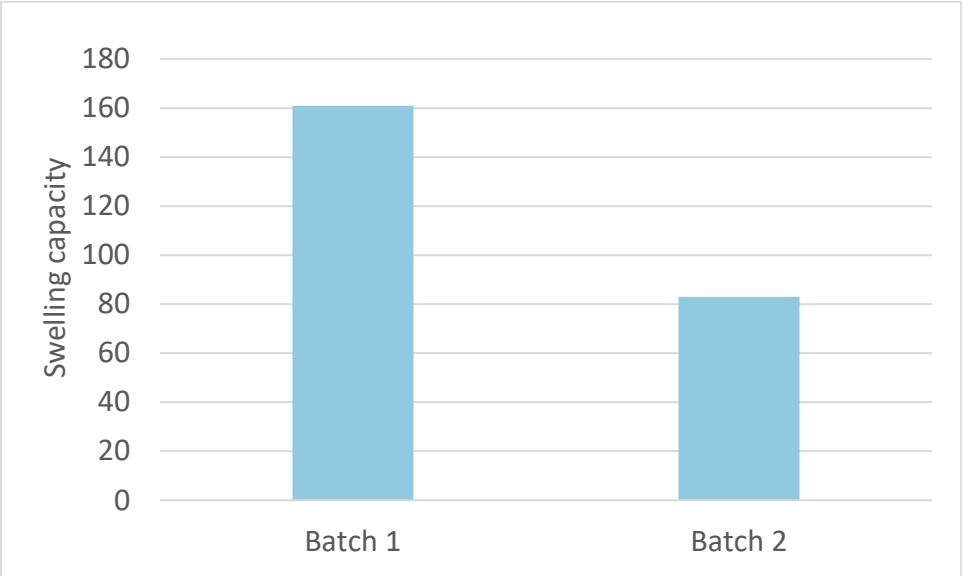

Figure 47: Average swelling capacity of samples from batch 1 and 2 in distilled water.

The average swelling capacity of the samples from batch 1 in distilled water was found to be significantly higher than the average swelling capacity of the samples from batch 2, on a 5 % significance level. The statistical data is summarised in Table E-13 of the appendix.

Figure 48: Samples from batch 1 after swelling in distilled water for one week.

Figure 49: Samples from batch 2 after swelling in distilled water for one week.

Figures 48 and 49 depict samples from batches 1 and 2 after swelling in distilled water for one week. As one can observe from the pictures, the samples from batch 1, with sample numbers from 1 to 5, were more deformed after the procedure than the samples from batch 2, with sample numbers from 6 to 10.

Batches 1 and 2 were prepared similarly, however, they have some differences. Firstly, the total monomer concentrations are 0.72 and 0.81 M, respectively. Higher monomer concentrations result in a higher amount of chemical bonds that binds the structure together. The mechanical strength the gel thus increases, which may explain why the samples from batch 2 were more intact than the samples from batch 1.

Secondly, there is also a small difference in the ratios of the concentration of crosslinker to concentration of total monomer with the ratio being 2.4 % in batch 1, and 2 % in batch 2. Higher concentrations of crosslinking polymers may increase the mechanical strength in batch 1, however, a difference of 0.4 % may not make a significant difference.

Thirdly, the concentration of APS in batch 1 was almost the double of what it was in batch 2. APS is an initiator, so more APS present could lead to more chain reactions going in parallel. It may also lead to more interaction between “growing” polymer-chains. Strong extension of the network give rise to defects in the form of chain breaks, which leads to an increase in swelling capacity. (64)

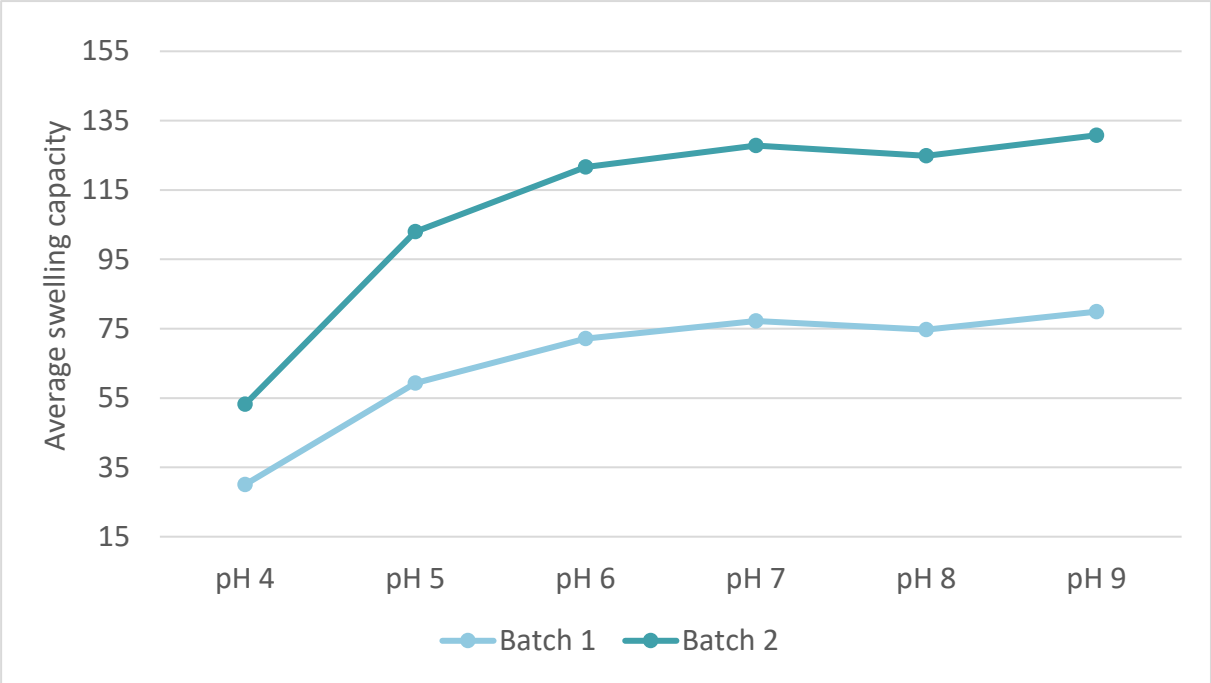

Figure 50: Plot of average swelling capacity for hydrogel samples from batch 1 and 2 in different Carmody solutions of pH-values from 4 to 9.

From Figures 50 and 51, one can observe a clear pH-dependency on the average swelling capacity (SC) in the pH-range from 4 to 7. Statistical tests at a 5 % significance level found that the average swelling capacities of batch 2 in solutions of pH 6, 7 and 8 were significantly higher than the corresponding average SCs of batch 1. In both batch 1 and 2, the average SC in pH 4 were also significantly lower than the average SCs in all other Carmody solutions.

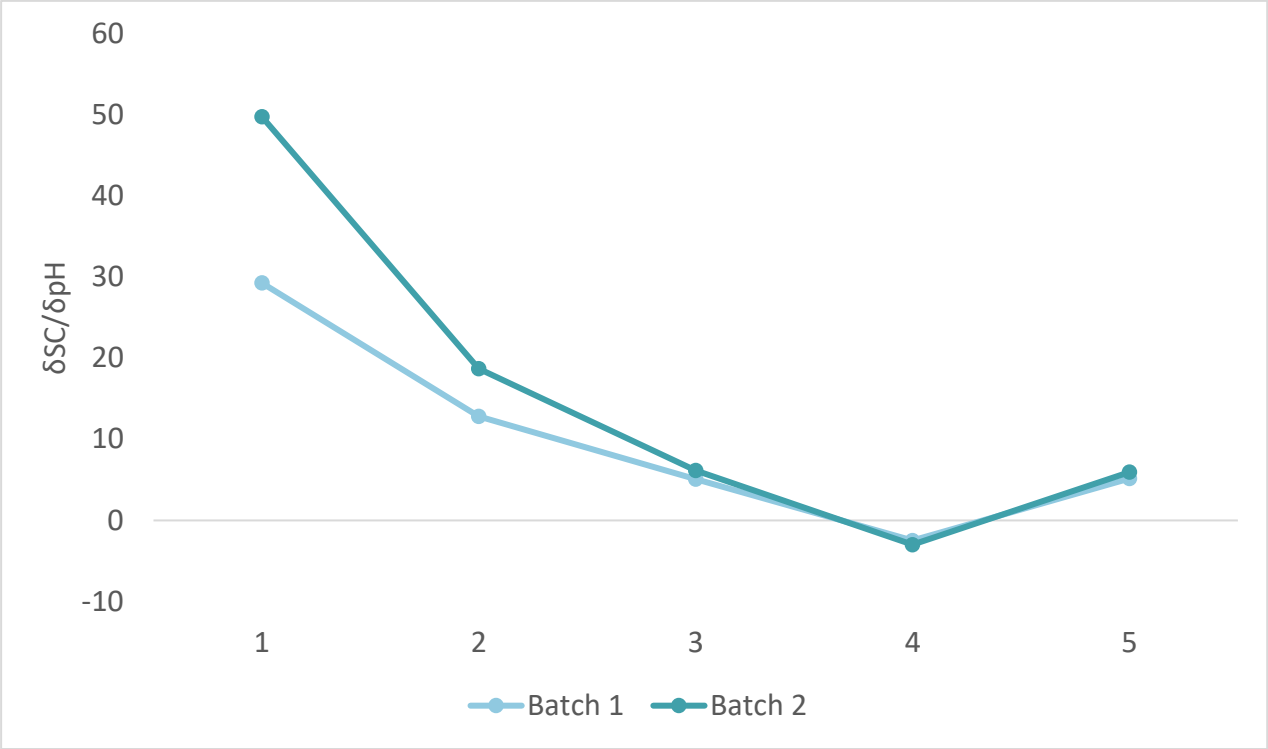

Figure 51: Derivative plot of figure 28. The y-axis is the change of the swelling constant over the change of pH. 1 on the x-axis corresponds to the interval from pH 4 to pH 5. 2, 3, 4 and 5 equivalently stands for intervals from pH 5-6, 6-7, 7-8, and 8-9.

Due to the more liquid-like state of the samples from batch 3 and 4, a dialysis tubing method was used to examine their swelling capacities. When samples from batch 3 and 4 were hydrated, they created slightly more viscous water solutions than pure water. It was first attempted to find the swelling capacity of samples from all batches with the same method as described under methods for batch 1 and 2. But this was found to be challenging for batch 3 and 4, where it was difficult to separate hydrogel from water. To confine the hydrogels while liquid could still come in contact and interact with the gels, samples of the gels were transferred to dialysis tubes via pipettes. This made more accurate measurements possible. The swelling capacities of batches 3 and 4 are calculated based on the hydrated weight of the samples. Therefore, they cannot be directly compared to the SCs of batches 1 and 2, which are calculated based on the dried sample weight.

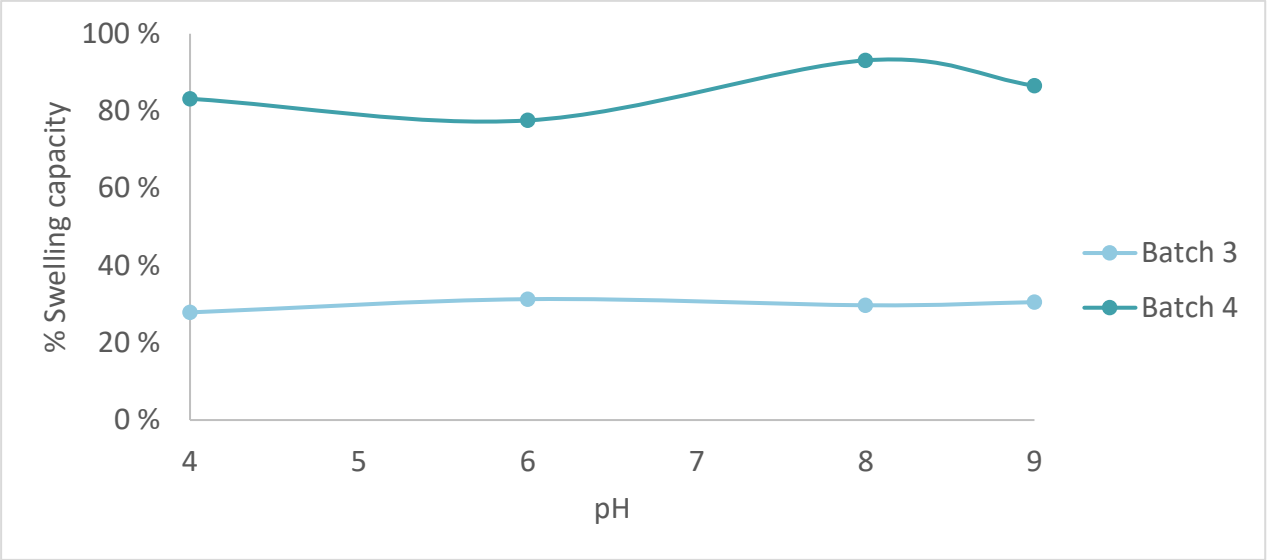

Figure 52: Plot of average swelling capacity in percent for hydrogel samples from batch 3 and 4 in Carmody solutions of pH 4, 6, 8 and 9.

One-way analysis of variance on a 5 % significance level determined that there was no significant difference between the swelling capacities of the samples in pH 4, 6, 8 or 9 for either batch 3 or 4 (Tables E-18 and 19). However, the average swelling capacities of batch 4 were found to be significantly higher than the average swelling capacities of batch 3 (Table E-20).

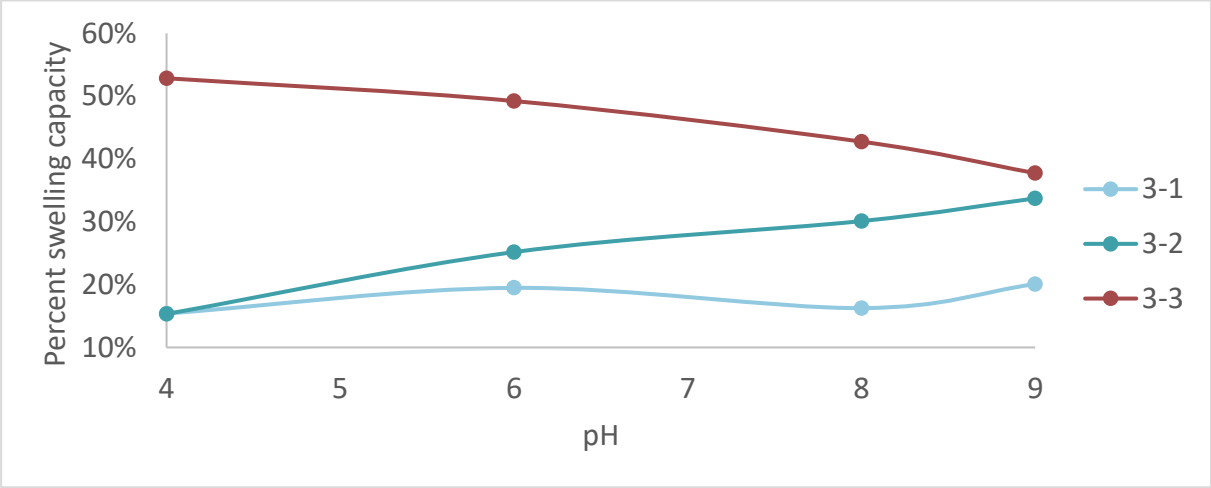

Figure 53: Plot of percent swelling capacities for hydrogel samples from batch 3 in Carmody solutions of pH 4, 6, 8 and 9.

Sample 3-3 contributes to a smaller average slope of the samples in batch 3, as shown in Figure 53.

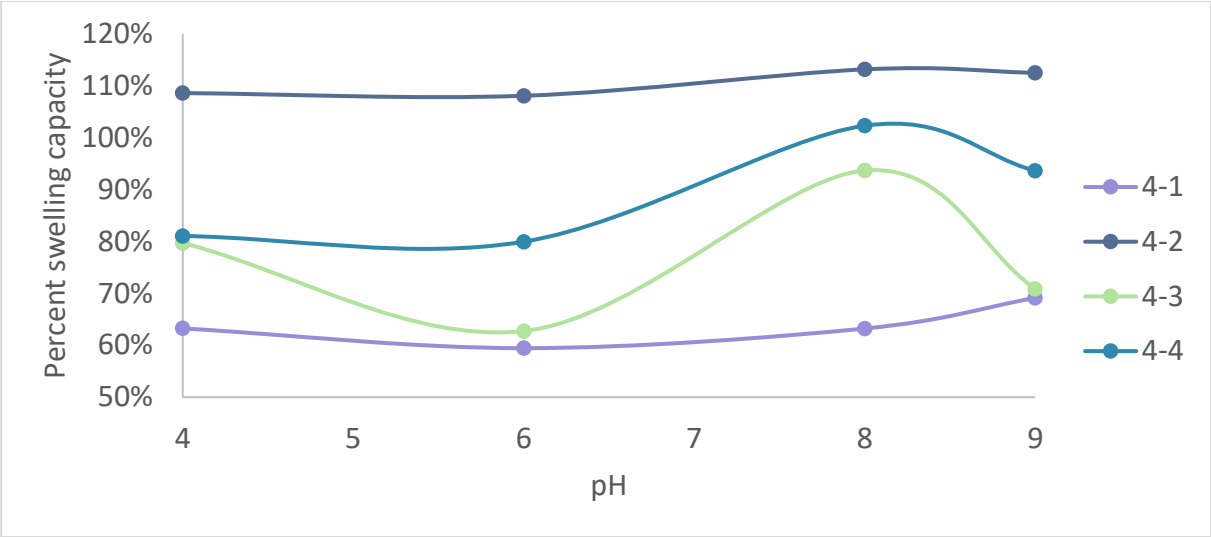

Figure 54: Plot of percent swelling capacities for hydrogel samples from batch 4 in Carmody solutions of pH 4, 6, 8 and 9.

Based on the statistical results and the plots in Figures 52-54, the hydrogels from batches 3 and 4 are not suitable for use as pH-sensing elements in an optical fibre sensor system. The hydrogels from batches 1 and 2 are more suitable for pH sensing in the pH range of 4 to 7, as shown in Figures 50 and 51. However, the statistical analysis indicates that the hydrogels from batches 1 and 2 are also not ideal for use as pH-sensing elements.

.

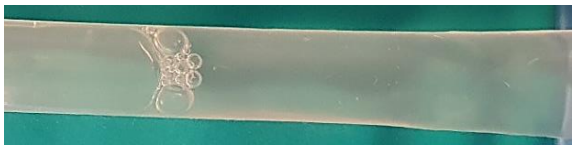

Figure 55: Sample from batch 3 after 48 hours in the pH 4 solution.

Figure 56: Same sample as in Figure 52, after 1 hour in the pH 9 solution (after 48 hours in pH 4 solution).

The hydrogel sample transitioned from collapsed state to swollen state in Figures 55 to 56, where the sample was transferred from a pH 4 solution to a pH 9 solution. All samples of batches 3 and 4 collapsed in the pH 4 solution. The dominant driving force for swelling in polyelectrolyte (i.e. charged) hydrogels is the inherent electrostatic repulsion between the gel charges. (65) If a change in the external environment of the gel, for example a change in pH, leads to effective attraction between the polymer links, then the gel collapses. (66)

There are several sources of error in the swelling capacity experiments. Firstly, the mass was not stable when the hydrogel samples were weighed. Liquid evaporated constantly from the surface of the gel samples and all samples could not be weighed simultaneously. To minimize this source of error, the samples were weighed in the same sequence each time, and the dialysis tube samples were dried and weighed one at a time. Secondly, the homogeneity of the samples is unknown. For example, the crosslinker bindings can be unevenly distributed, consequently, samples taken from the same hydrogel are not homogeneous and may increase the variation of the results.

3.2.2 Observations and discussion of physical properties

The physical properties of the hydrogels were not entirely ideal for their intended use. While elasticity was a positive physical property observed, the tensile strength of the gels was unsatisfactory, as they were brittle and broke in pieces quite easily. The concentration of crosslinker in the hydrogels affects their physical properties. With too low concentrations of added BIS, the hydrogel will be water soluble and will not “set”. (67) The concentrations of BIS in the hydrogels produced in batch 3, 4 and 5 likely were too low as the gels were very liquid-like when hydrated. The hydrogels of batch 5, which had the lowest concentration of BIS, did not “set” and remained liquid-like even when not hydrated.

On the other side, too high crosslinker concentrations can lead to a poor degree of swelling. Advantages of higher concentrations of crosslinking polymers include increased mechanical strength and greater resistance to heat, wear, and attack by solvents. (49) The degree of swelling does not need to be very high, provided that the adsorption between the hydrogel and the optical fibre is adequate for detectable strain. However, materials with lower crosslink

densities typically exhibit higher adhesiveness to surfaces compared to those with higher crosslink densities. (61) The adhesion of the hydrogels to the surface of optical fibres has not been tested in this thesis and may pose a challenge for these gels. In future experiments, it would be valuable to find the optimal concentration of BIS and to examine the adhesion of the gels to optical fibre coating materials. If the mechanical strength of the gels is not satisfactory, even with an optimal concentration of BIS, it may be necessary to add a strengthening material. Carbon-based materials, such as graphene, carbon nanotubes, and carbon nanofibres, can act as reinforcing agents when incorporated into hydrogels, providing structural integrity and strength to the gel network. (68,69)

The Schlenk line removed possible oxygen gas and replaced it with the inert gas argon throughout the preparation process. The degasification through ultrasonication and bubbling with nitrogen gas replaced the gas in the solutions with nitrogen gas. The main difference between the two methods is that one is a closed system, and the other is open. In both methods, solutions set, and hydrogels were produced. It is assumed that the Schlenk line will provide a better environment for the controlled initialization of the polymerization process. Unfortunately, the differences in amount of crosslinker makes it difficult to directly compare the effect of different reaction set-up on the properties of the formed hydrogels. To compare the two degasification methods effects on the properties of the gels, in further experiments, batches with otherwise identical preparations and concentrations could be prepared with each method of degasification.

3.3 Discussion regarding both sensor-systems

pH-measurements of all Carmody buffer solutions used in the experiments are found in chapter E of the appendix. All pH-values are measured to be approximately 0.5 lower than the wanted pH-value. That all pH-measurements were lower than the aimed at pH-value suggests that there was a systematic error in the preparations of the solutions and/or in the pH-meter. Since the measurements showed the same trend and would only shift the plots, the pH-values in the plots have not been replaced with the measured values. However, they are all listed in the appendix.

Acridine has favourable properties as the fluorophore in fluorescence lifetime-based pH-sensors. Most dyes have lifetimes under 1.0 ns over the pH-range of 6.0 to 8.0, while acridine can exhibit a fluorescence lifetime from around 10 ns to 31 ns. (27) Ryder et al. found that acridine had the largest lifetime variation of 12.5 ns over the pH-range of 5.8 to 8. Due to this, it is expected that acridine will give a pH-sensor better sensitivity in that range compared with fluorophores with shorter lifetime variations. Conversely, shorter FL variation means that the doped segments can be placed with smaller gaps in between the segments on an optical fibre cable, which would increase accuracy of the sensor.

Based on the fluorescence lifetime pH-variability of acridine, the pH-range of the route with acridine as the sensing element would likely be from pH 6 to 8. The optical power monitor experiments of the acridine-doped optical fibre in Carmody solutions ranging from pH 4 to 9, did not result in significant pH-sensing. Further experiments should explore the fluorescence and fluorescence lifetime variations in different pH-environments. The route that has been explored with hydrogels as sensing elements showed some potential for sensing in the range from pH 4 to 7, however, the results were not statistically significant. Among these two routes, the fluorescence lifetime-based pH sensor with acridine as the sensing element shows the most promise and is the most interesting for further investigation.

4. Conclusions

The aim of the thesis was to test and apply pH-sensitive materials for interaction with optical fibres. This objective has been achieved by exploring two routes of pH-sensitive materials as sensing elements in optical fibre pH-sensor systems.

In the first route, acridine was used as the sensing element. An optimal method for removing the nylon coating from optical fibres was documented, and the silicone cladding of plastic-clad silica was successfully doped with acridine. However, optical power monitoring experiments of acridine-doped optical fibres in Carmody solutions with pH values ranging from 4 to 9 did not yield statistically significant results for pH sensing at a 5% significance level. Further experiments should explore the fluorescence and fluorescence lifetime variations of acridine in different pH environments.

In the second route, hydrogels were explored as pH-sensitive materials for use as sensing elements in strain-based optical fibre pH sensors. Five batches of hydrogels were prepared. The swelling capacities of the gels in batches 1 and 2 showed potential for pH-sensing in the range of 4 to 7. However, statistical tests indicated that the results were not significantly different at a 5% significance level, rendering the hydrogels unsuitable for their intended use as sensing elements. Future experiments should aim to improve the properties of the hydrogels, for example, by optimizing the concentration of BIS. Additionally, future experiments should explore the adhesion of the gels to optical fibre coating materials.

Among the two routes investigated, the fluorescence lifetime-based pH sensor with acridine as the sensing element shows the most promise and is the most interesting for further investigation.

5. References

1. Acid–base reaction - Theories, Definitions, Properties | Britannica [Internet]. [cited 2024 Jun 3]. Available from: https://www.britannica.com/science/acid-base-reaction

2. What is the significance of pH in acid-base reactions? | TutorChase [Internet]. [cited 2024 Apr 24]. Available from: https://www.tutorchase.com/answers/igcse/chemistry/what-is-the-significance-of-ph-in-acid-base-reactions

3. Myers R. One-Hundred Years of pH. J Chem Educ - J CHEM EDUC. 2009 Dec 18;87.

4. Science History Institute [Internet]. [cited 2023 Dec 13]. Arnold O. Beckman. Available from: https://www.sciencehistory.org/education/scientific-biographies/arnold-o-beckman/

5. Reynolds J. A Breakdown of the Uses of pH in Different Industries [Internet]. [cited 2024 Apr 24]. Available from: https://blog.jencoi.com/a-breakdown-of-the-uses-of-ph-in-different-industries

6. pH Sensing | Ocean Insight [Internet]. [cited 2023 Dec 12]. Available from: https://www.oceaninsight.com/knowledge-hub/measurement-techniques/ph-sensing/

7. Baldini F. Critical review of pH sensing with optical fibers. Proc SPIE - Int Soc Opt Eng. 1999 Feb 23;3540.

8. Yin S, Ruffin P, Yu F. Fiber Optic Sensors. In: Second Edition. CRC Press; p. 2.

9. Rudolf Seitz W. New directions in fiber optic chemical sensors: Sensors based on polymer swelling. J Mol Struct. 1993 Mar 1;292:105–13.

10. Totland C, Thomas P, Størdal I, Eek E. A Fully Distributed Fibre Optic Sensor for the Detection of Liquid Hydrocarbons. IEEE Sens J. 2020 Dec 25;PP:1–1.

11. Design and fabrication of polymer nanocomposite sensors - ScienceDirect [Internet]. [cited 2024 Mar 5]. Available from: https://www.sciencedirect.com/science/article/abs/pii/B9780323988308000084

12. Abdul S, Judit T, Ilona F, Nikoletta M. Chapter 16 - Functional thin films and nanostructures for sensors. In: Barhoum A, Hamdy Makhlouf AS, editors. Fundamentals of Nanoparticles [Internet]. Elsevier; 2018 [cited 2024 Mar 5]. p. 485–519. (Micro and Nano Technologies). Available from: https://www.sciencedirect.com/science/article/pii/B9780323512558000161

13. Lu X, Thomas PJ, Hellevang JO. A Review of Methods for Fibre-Optic Distributed Chemical Sensing. Sensors. 2019 Jan;19(13):2876.

14. Photonics.com [Internet]. [cited 2024 May 25]. Definition of fluorophore. Available from: https://www.photonics.com/EDU/fluorophore/d4193

15. Totland C, Thomas PJ, Holst B, Akhtar N, Hovdenes J, Skodvin T. A Broad-Range Fluorescence Lifetime pH Sensing Material Based on a Single Organic Fluorophore. J Fluoresc. 2019 Sep 1;29(5):1125–31.

16. Gerlach G, Guenther M, Suchaneck G, Sorber J, Arndt KF, Richter A. Application of sensitive hydrogels in chemical and pH sensors. Macromol Symp. 2004 Mar 1;210:403–10.

17. Shakhsher Z, Seitz WR, Legg KD. Single fiber-optic pH sensor based on changes in reflection accompanying polymer swelling. Anal Chem. 1994 May 15;66(10):1731–5.

18. Lavine BK, Pampati SR, Dahal KS, Kim M, Perera UDNT, Benjamin M, et al. Swellable Copolymers of N-isopropylacrylamide and Alkyl Acrylic Acids for Optical pH Sensing. Molecules. 2020 Mar 19;25(6):1408.

19. Zhang Z, Shakhsher Z, Seitz WR. Aminated polystyrene membranes for a fiber optic pH sensor based on reflectance changes accompanying polymer swelling. Mikrochim Acta. 1995 Mar 1;121:41–50.

20. Potyrailo R, Hieftje G. Use of the original silicone cladding of an optical fiber as a reagent-immobilization medium for intrinsic chemical sensors. Fresenius J Anal Chem. 1999 May 11;364:32–40.

21. Scorsone E, Christie S, Persaud K, Kvasnik F. Evanescent sensing of alkaline and acidic vapours using a plastic clad silica fibre doped with poly(o-methoxyaniline). Sens Actuators B-Chem - Sens ACTUATOR B-CHEM. 2004 Feb 1;97:174–81.

22. Evaluation of Acridine in Nafion as a Fluorescence-Lifetime-Based pH Sensor [Internet]. [cited 2024 May 23]. Available from: https://journals.sagepub.com/doi/epdf/10.1366/00037020332116523 2?src=getftr

23. A fully distributed fibre optic sensor for relative humidity measurements - ScienceDirect [Internet]. [cited 2024 Apr 26]. Available from: https://www.sciencedirect.com/science/article/abs/pii/S0925400517302472

24. Lakowicz JR, editor. Principles of Fluorescence Spectroscopy [Internet]. Boston, MA: Springer US; 2006 [cited 2024 Jan 26]. Available from: https://link.springer.com/10.1007/978-0-387-46312-4

25. Fluorescence | Emission, Excitation & Photochemistry | Britannica [Internet]. [cited 2024 Feb 2]. Available from: https://www.britannica.com/science/fluorescence

26. Fluorescence Lifetime Measurement [Internet]. [cited 2024 Jan 16]. Available from: https://www.sigmaaldrich.com/NO/en/technical-documents/technical-article/cell-culture-and-cell-culture-analysis/imaging-analysis-and-live-cell-imaging/fluorescence-lifetime-measurement

27. Ryder A, Power S, Glynn T, Morrison J. Time-domain measurement of fluorescence lifetime variation with pH. In 2001. p. 102–9.

28. Everything You Need To Know About Fibre Optic Cables | RS [Internet]. [cited 2024 Feb 14]. Available from: https://au.rs-online.com/web/generalDisplay.html?id=ideas-and-advice/fibre-optic-cables-guide

29. Thompson RB. Fluorescence-Based Fiber-Optic Sensors. In: Lakowicz JR, editor. Topics in Fluorescence Spectroscopy: Principles [Internet]. Boston, MA: Springer US; 2002 [cited 2024 Apr 25]. p. 345–65. Available from: https://doi.org/10.1007/0-306-47058-6_7

30. Networking [Internet]. [cited 2024 Feb 21]. What Is Fiber Optics? Definition from SearchNetworking. Available from: https://www.techtarget.com/searchnetworking/definition/fiber-optics-optical-fiber

31. Fiber optics | Definition, Inventors, & Facts | Britannica [Internet]. 2024 [cited 2024 Feb 21]. Available from: https://www.britannica.com/science/fiber-optics

32. Optical Power In Optical Fiber [Internet]. 2022 [cited 2024 May 30]. Available from: https://fiberopticx.com/optical-power/

33. Park H, Guo X, Temenoff JS, Tabata Y, Caplan AI, Kasper FK, et al. Effect of swelling ratio of injectable hydrogel composites on chondrogenic differentiation of encapsulated rabbit marrow mesenchymal stem cells in vitro. Biomacromolecules. 2009 Mar 9;10(3):541–6.

34. Hydrogels from polysaccharide-based materials: Fundamentals and applications in regenerative medicine. In: Natural-Based Polymers for Biomedical Applications [Internet]. Woodhead Publishing; 2008 [cited 2024 Mar 25]. p. 485–514. Available from: https://www.sciencedirect.com/science/article/abs/pii/B9781845692643500184

35. Kocak G, Tuncer C, Bütün V. pH-Responsive polymers. Polym Chem. 2017;8(1):144–76.

36. Bajpai AK, Shukla S, Bhanu S, Kankane S. Responsive Polymers in Controlled Drug Delivery. Prog Polym Sci. 2008 Nov 1;33:1088–118.

37. Sievers J, Sperlich K, Stahnke T, Kreiner C, Eickner T, Martin H, et al. Determination of hydrogel swelling factors by two established and a novel non-contact continuous method. J Appl Polym Sci. 2021;138(18):50326.

38. Carmody WR. Easily prepared wide range buffer series. J Chem Educ. 1961 Nov 1;38(11):559.

39. Sörensen SPL. Über die Messung und Bedeutung der Wasserstoffionen-konzentration bei biologischen Prozessen. Ergeb Physiol. 1912 Dec 1;12(1):393–532.

40. Clark WM, Lubs HA. HYDROGEN ELECTRODE POTENTIALS OF PHTHALATE, PHOSPHATE, AND BORATE BUFFER MIXTURES. J Biol Chem. 1916 Jul 1;25(3):479–510.

41. Prideaux EBR, Ward AT. LI.—Calculations on the neutralisation of mixtures of acids, and a universal buffer mixture. J Chem Soc Trans. 1924 Jan 1;125(0):426–9.

42. McIlvaine TC. A BUFFER SOLUTION FOR COLORIMETRIC COMPARISON. J Biol Chem. 1921 Nov 1;49(1):183–6.

43. Kipcak AS, Ismail O, Doymaz I, Piskin S. Modeling and Investigation of the Swelling Kinetics of Acrylamide-Sodium Acrylate Hydrogel. J Chem. 2014 Aug 13;2014:e281063.

44. Free Radical Vinyl Polymerization [Internet]. Polymer Science Learning Center; [cited 2024 Jan 10]. Available from: https://pslc.ws/macrog/radical.htm

45. Specialty Chemicals home pages | FUJIFILM Wako Chemicals Europe GmbH [Internet]. 2022 [cited 2024 Jan 10]. Specialty Chemicals home pages | FUJIFILM Wako Chemicals Europe GmbH. Available from: https://specchem-wako.fujifilm.com/europe/en/

46. BYJUS [Internet]. [cited 2024 Mar 18]. Free Radical Polymerization - Introduction, Mechanism, Thermodynamics and Applications of Free Radical Polymerization. Available from: https://byjus.com/chemistry/free-radical-polymerization/

47. TEMED [Internet]. Tiaris Biosciences. 2023 [cited 2024 Feb 14]. Available from: https://tiarisbiosciences.com/temed/

48. Menter P. Acrylamide Polymerization — A Practical Approach.

49. Maitra J, Shukla VK. Cross-linking in Hydrogels - A Review. Am J Polym Sci. 2014;4(2):25–31.

50. Compare the Difference Between Similar Terms [Internet]. 2021 [cited 2024 Mar 18]. Difference Between Physical and Chemical Cross Linking. Available from: https://www.differencebetween.com/difference-between-physical-and-chemical-cross-linking/

51. Siqueira E, França J, Souza R, Leoterio D, Cordeiro J, Bogdan D. Mecanisms of the chemical crosslinking to obtain the hydrogels: Synthesis, conditions of crosslinking and biopharmaceutical applications. Res Soc Dev. 2023 Sep 1;12:e18312943072.

52. Kishore K, Bhanu VA. Effect of oxygen on the polymerization of acrylamide. J Polym Sci Part Polym Chem. 1986;24(2):379–81.

53. Ultrasonics | Physics, Sound Waves & Applications | Britannica [Internet]. 2023 [cited 2024 Feb 2]. Available from: https://www.britannica.com/science/ultrasonics

54. Leong T, Ashokkumar M, Kentish S. The Growth of Bubbles in an Acoustic Field by Rectified Diffusion. In: Handbook of Ultrasonics and Sonochemistry [Internet]. Singapore: Springer; 2016 [cited 2024 Feb 2]. p. 69–98. Available from: https://doi.org/10.1007/978-981-287-278-4_74

55. Asakura Y, Yasuda K. Frequency and power dependence of ultrasonic degassing. Ultrason Sonochem. 2022 Jan 1;82:105890.

56. Schlenk Line: Fundamentals [Internet]. [cited 2024 Apr 3]. Available from: https://www.learnsci.com/resources/schlenk-line-fundamentals

57. Hickman D. Tips and Tricks for the Lab: Air-Sensitive Techniques (2) [Internet]. ChemistryViews. 2013 [cited 2024 Apr 3]. Available from: https://www.chemistryviews.org/details/education/4308331/Tips_and_Tricks_for_the_Lab_Air-Sensitive_Techniques_2/

58. Webb P. 5.3 Salinity Patterns. [cited 2024 May 29]; Available from: https://rwu.pressbooks.pub/webboceanography/chapter/5-3-salinity-patterns/

59. PubChem. Propylene Glycol [Internet]. [cited 2023 Sep 26]. Available from: https://pubchem.ncbi.nlm.nih.gov/compound/1030

60. Ryan ET, Xiang T, Johnston KP, Fox MA. Absorption and Fluorescence Studies of Acridine in Subcritical and Supercritical Water. J Phys Chem A. 1997 Mar 1;101(10):1827–35.

61. Scales CW, Popwell S, Pall B, Johnson B, Maggio T. Sticky Business: How Cross-Linker Content Can Have a Profound Effect on the Adhesiveness of Contact Lenses. Invest Ophthalmol Vis Sci. 2017 Jun 23;58(8):3094.

62. Kabiri K, Omidian H, Hashemi SA, Zohuriaan-Mehr MJ. Synthesis of fast-swelling superabsorbent hydrogels: effect of crosslinker type and concentration on porosity and absorption rate. Eur Polym J. 2003 Jul 1;39(7):1341–8.

63. Polymer_Coatings_for_Silica_Optical_Fiber_Nov_2009.pdf [Internet]. [cited 2024 Jan 15]. Available from: https://www.molex.co.in/content/dam/molex/molex-dot-com/en_us/pdf/product-reference-guides/polymicro/white-papers/Polymer_Coatings_for_Silica_Optical_Fiber_Nov_2009.pdf?inline

64. Bel'nikevich N, Bobrova N, Elokhovskiy V, Zoolshoev Z, Smirnov M, Elyashevich G. Effect of Initiator on the Structure of Hydrogels of Cross-Linked Polyacrylic Acid. Russ J Appl Chem. 2011 Dec 1;84.

65. Ostroha J, Pong M, Lowman A, Dan N. Controlling the collapse/swelling transition in charged hydrogels. Biomaterials. 2004 Aug 1;25(18):4345–53.

66. collapse of polymer gels [Internet]. [cited 2024 Jun 3]. Available from: https://eng.thesaurus.rusnano.com/wiki/article2159

67. Nasution H, Harahap H, Dalimunthe NF, Ginting MHS, Jaafar M, Tan OOH, et al. Hydrogel and Effects of Crosslinking Agent on Cellulose-Based Hydrogels: A Review. Gels. 2022 Sep 7;8(9):568.

68. Hussain S, Maktedar SS. Structural, functional and mechanical performance of advanced Graphene-based composite hydrogels. Results Chem. 2023 Dec 1;6:101029.

69. Ferreira HP, Moura D, Pereira AT, Henriques PC, Barrias CC, Magalhães FD, et al. Using Graphene-Based Materials for Stiff and Strong Poly(ethylene glycol) Hydrogels. Int J Mol Sci. 2022 Feb 19;23(4):2312.

70. Hard-Coated Edgepass Filters [Internet]. [cited 2024 Jan 18]. Available from: https://www.thorlabs.com

71. Fluorescence Imaging Filters [Internet]. [cited 2024 Jan 18]. Available from: https://www.thorlabs.com

72. Hard-Coated Edgepass Filters [Internet]. [cited 2024 Jan 18]. Available from: https://www.thorlabs.com

73. Hard-Coated UV/VIS Bandpass Filters [Internet]. [cited 2024 May 11]. Available from: https://www.thorlabs.com

Appendix

A. Transmission data of selected optical filters

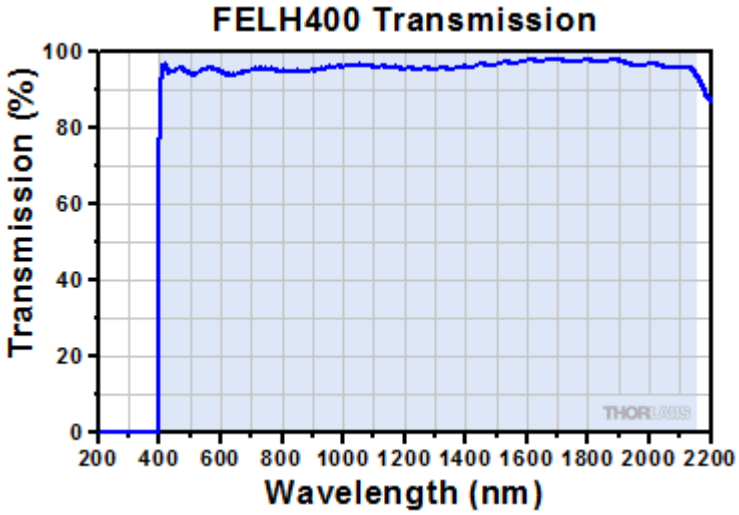

Figure A-1: Transmission data of the FELH400 filter, adapted from Thorlabs. (70) The shaded region in the graph represents the FELH400 filter's region of transmission, which is from 407 to 2150 nm. This filter is a long pass filter with cut-on wavelength at 400 nm. The x-axis is wavelength in nanometres, and the y-axis is transmission in percent.

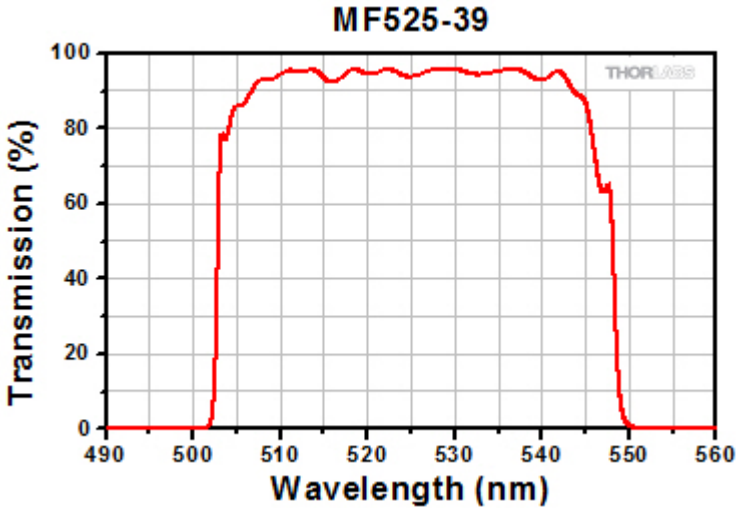

Figure A-2: Transmission range of the MF252-39 emission filter, adapted from Thorlabs. (71) The x-axis is wavelength in nanometres, and the y-axis is transmission in percent. The filter has over 90 % transmission between 505.5 nm and 544.5 nm and transmits below 0.001 % at other wavelengths.

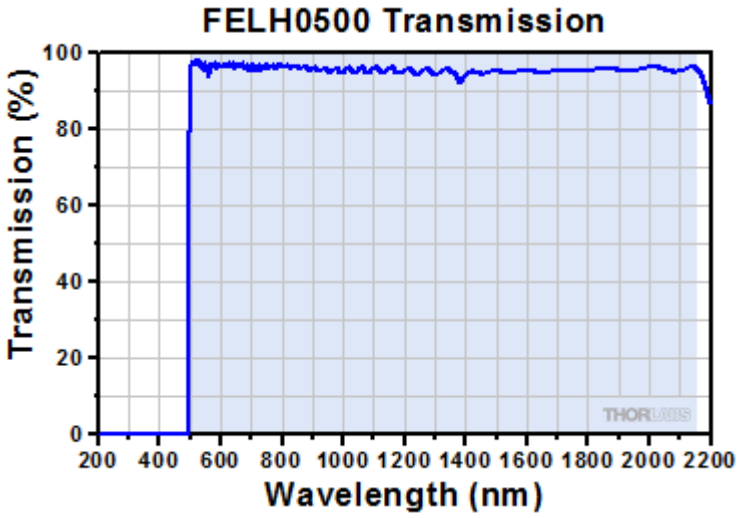

Figure A-3: Transmission data of the FELH0500 optical filter, adapted from Thorlabs. (72) The shaded region in the graph represents the FELH0500 filter's region of transmission, which is from 508 to 2150 nm. The filter is a long pass filter with cut-on wavelength at 500 nm. The x-axis is wavelength in nanometres, and the y-axis is transmission in percent.

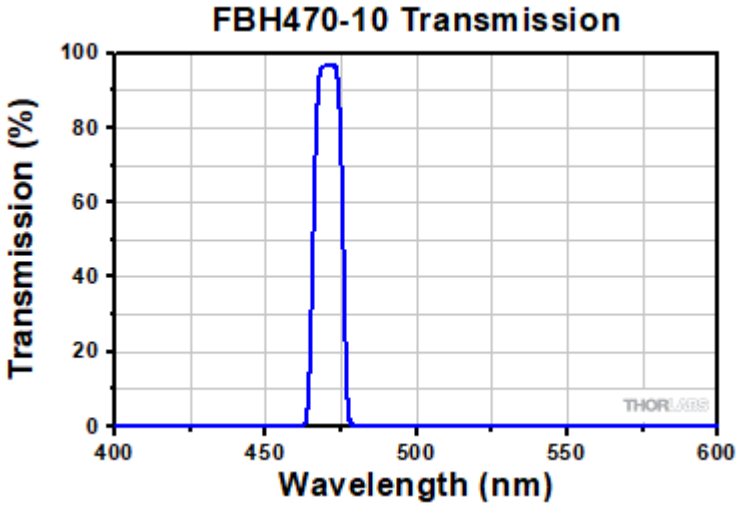

Figure A-4: Transmission data of the FBH470-10 optical filter, adapted from Thorlabs. (73) The x-axis is wavelength in nanometres, and the y-axis is transmission in percent. FBH470-10 is a hard-coated bandpass filter with central wavelength at 470 nm and full width at half maximum of 10 nm.

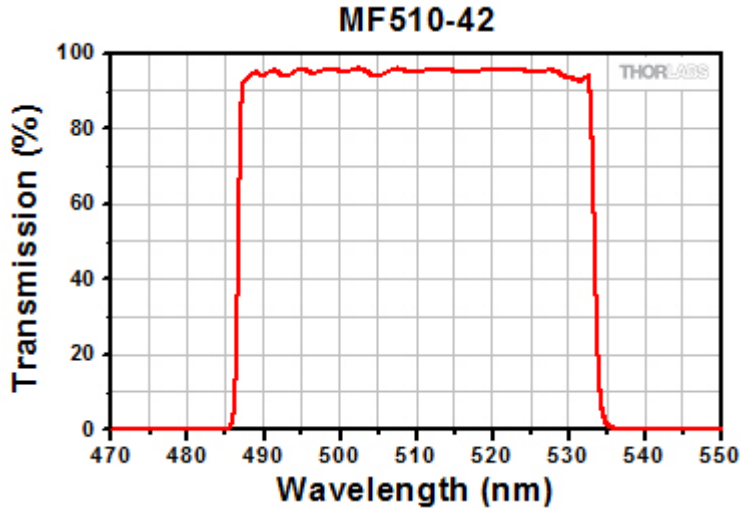

Figure A-5: Transmission data of the MF510-42 filter, adapted from Thorlabs. (71) The x-axis is wavelength in nanometres, and the y-axis is transmission in percent. MF510-42 is a fluorescence emission filter with central wavelength of 510 nm and band width of 42 nm.

B. Data from optical power monitor experiments

Table B-1: Minimum and maximum measured optical power in microwatt transmitted through the optical fibre cables with and without the application of optical filters.

	Minimum measured optical power [µW]	**Maximum measured optical power [µW]**
Doped OFC without optical filter	768	790
Undoped OFC without optical filter	1672	1678
Doped OFC with FELH0500 filter	0.299	0.317
Undoped OFC with FELH0500 filter	0.257	0.268
Doped OFC with FELH400 filter	5.28	5.33
Undoped OFC with FELH400 filter	7.95	7.98
Doped OFC with MF525-39 filter	0.088	0.114
Undoped OFC with MF525-39 filter	0.073	0.091

C. Additional plots from optical power monitoring of acridine-doped cladding in Carmody buffer solutions

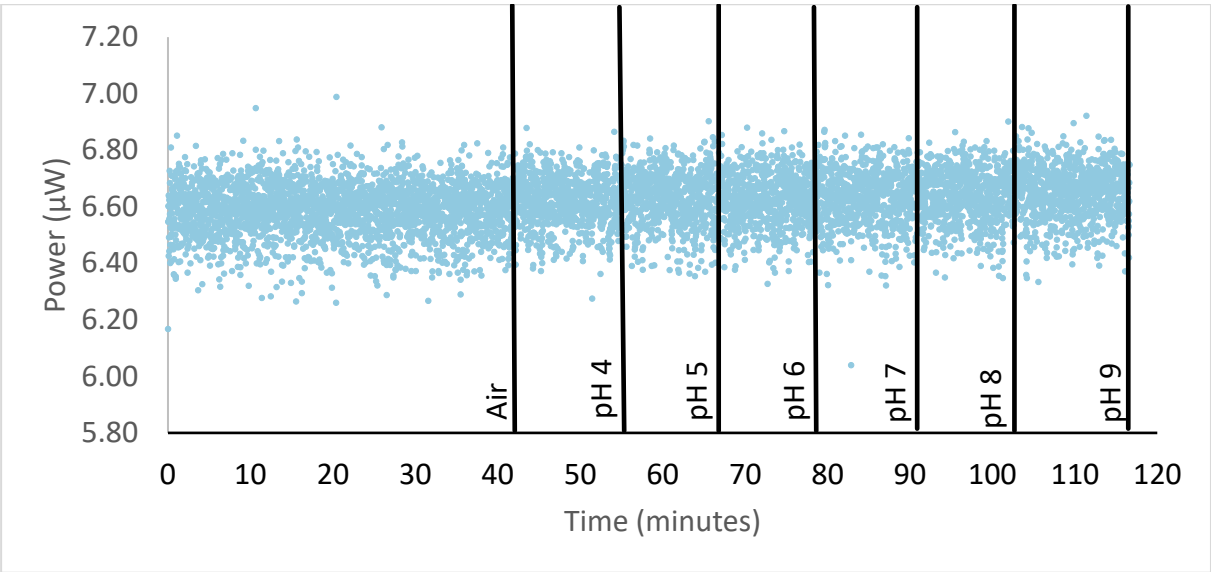

Figure C-1: Car-1, power in microwatts plotted against time in minutes. Continuous measurement of optical power transmitted while doped-cladding is in Carmody solutions of increasing pH-values. Linear trendline of the samples gave the function y= 0.0006x + 6.5795.

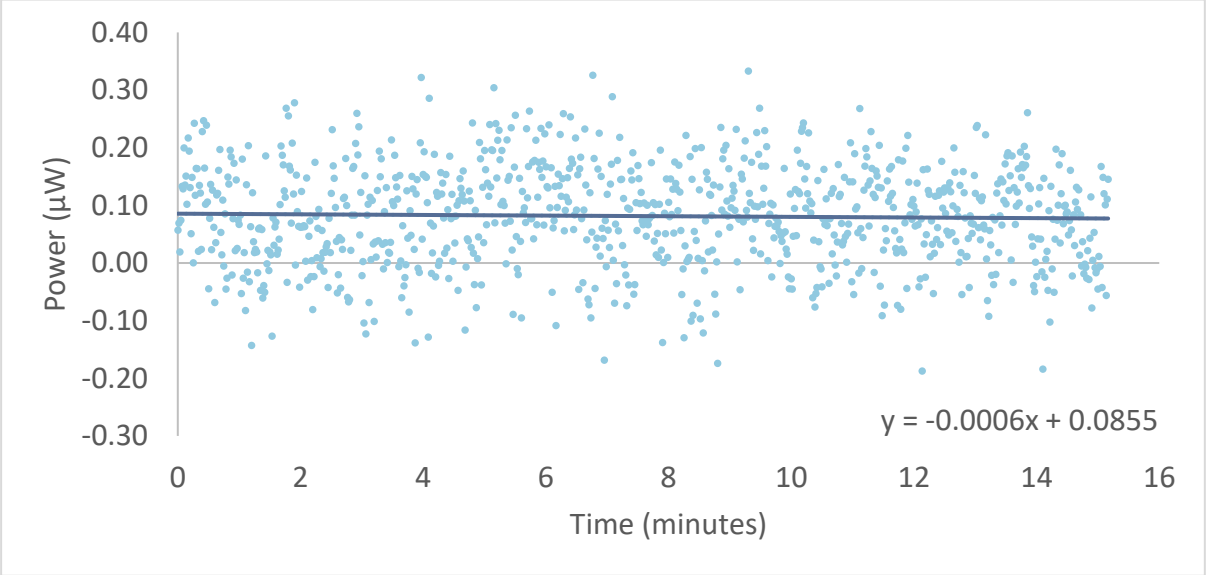

Figure C-2: Car- 2, optical power transmitted in microwatts plotted against time in minutes. Dry cladding in air with FB470-10 optical filter attached in set-up. Linear trend line of the samples gave the function y = -0.0006x + 0.0855.

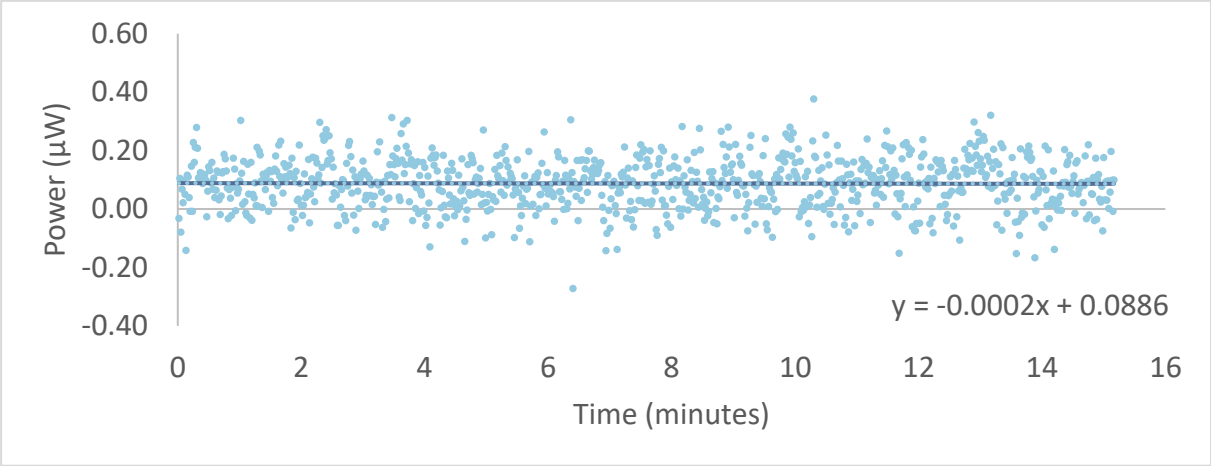

Figure C-3: Car-2, optical power transmitted in microwatts plotted against time in minutes. FB470-10 optical filter attached in set-up and cladding laying in a Carmody solution of pH 4. Linear trend line of the samples gave the function y = -0.0002x + 0.0886.

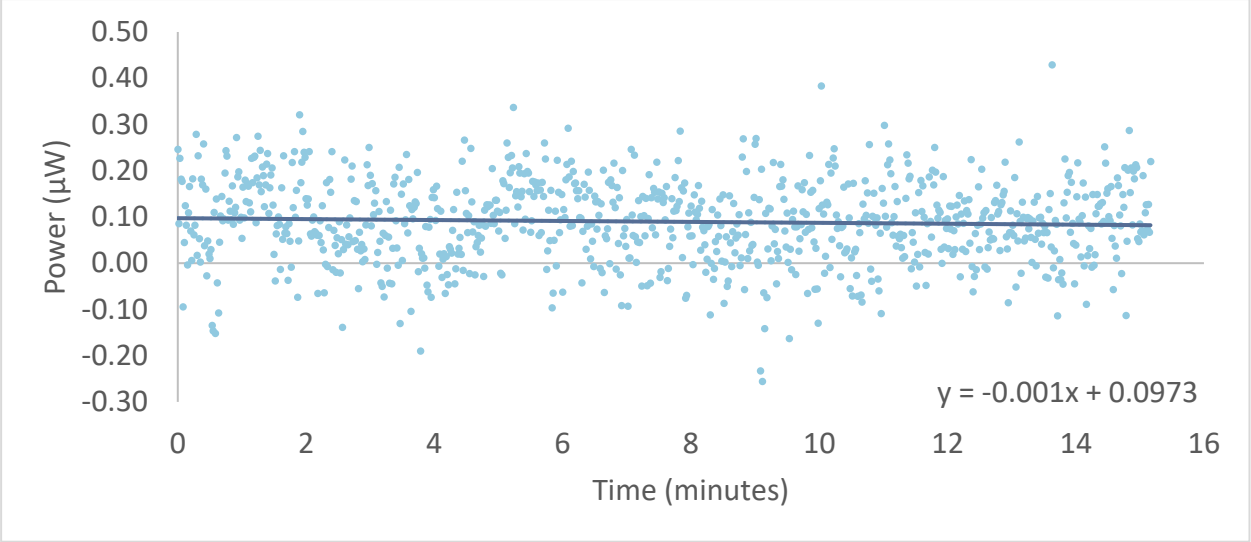

Figure C-4: Car-2, optical power transmitted in microwatts plotted against time in minutes. FB470-10 optical filter attached in set-up and cladding laying in a Carmody solution of pH 6. Linear trend line of the samples gave the function y = -0.0001x + 0.0973.

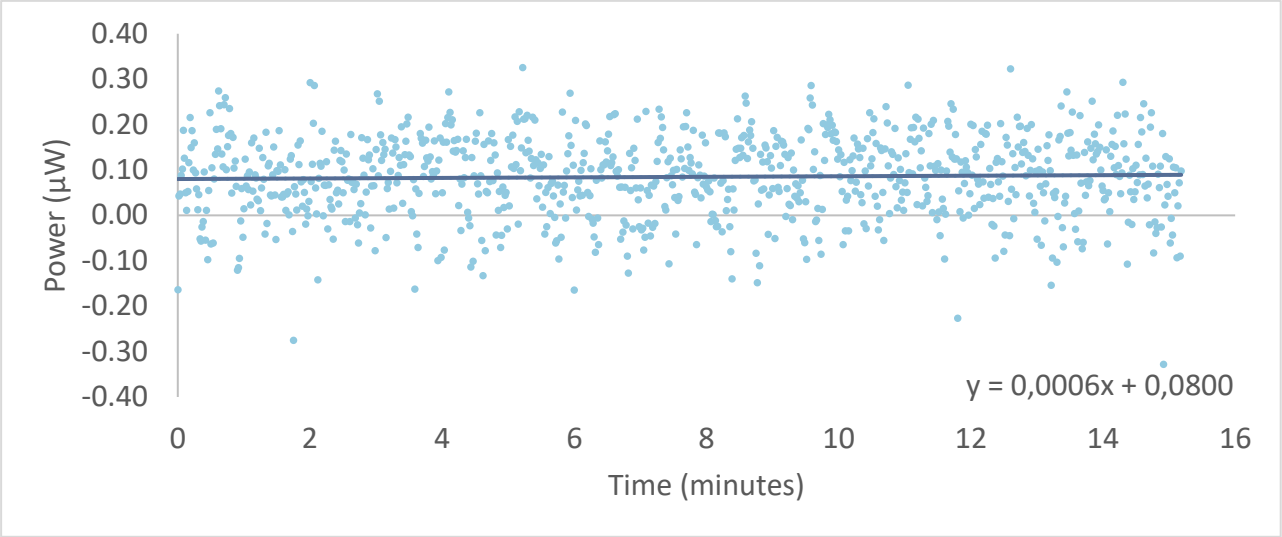

Figure C-5: Car-2, optical power transmitted in microwatts plotted against time in minutes. FB470-10 optical filter attached in set-up and cladding laying in a Carmody solution of pH 9. Linear trend line of the samples gave the function y = 0.0006x + 0.0800.

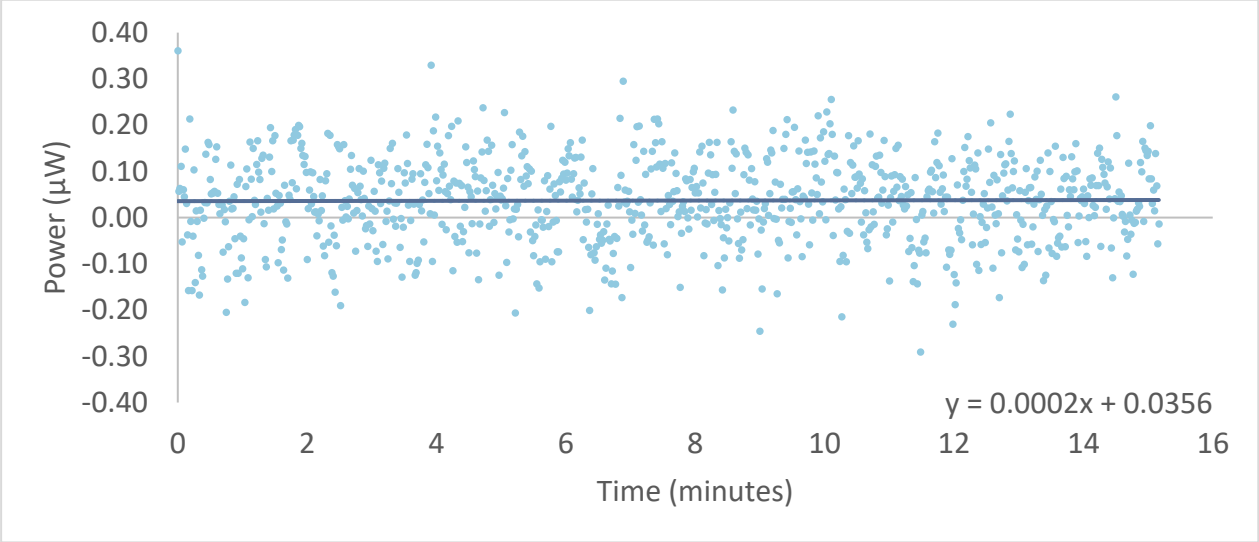

Figure C-6: Car-3, optical power transmitted in microwatts plotted against time in minutes. MF510-42 optical filter attached in set-up and cladding laying in a Carmody solution of pH 4. Linear trend line of the samples gave the function y = 0.0002x + 0.0356.

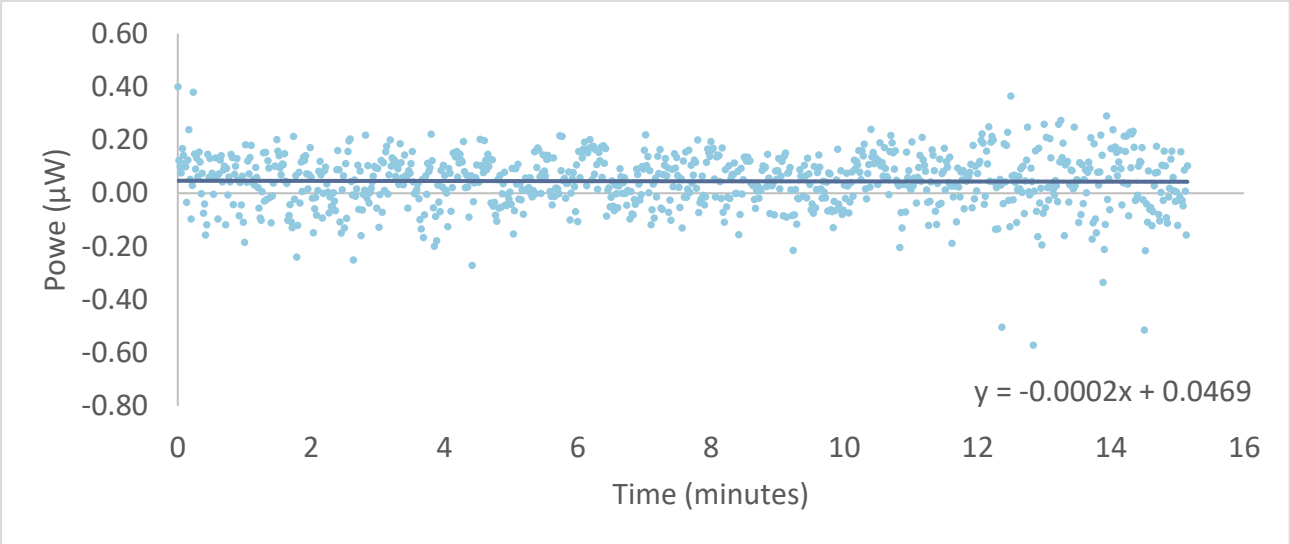

Figure C-7: Car-3, optical power transmitted in microwatts plotted against time in minutes. MF510-42 optical filter attached in set-up and cladding laying in a Carmody solution of pH 6. Linear trend line of the samples gave the function y = -0.0002x + 0.0469.

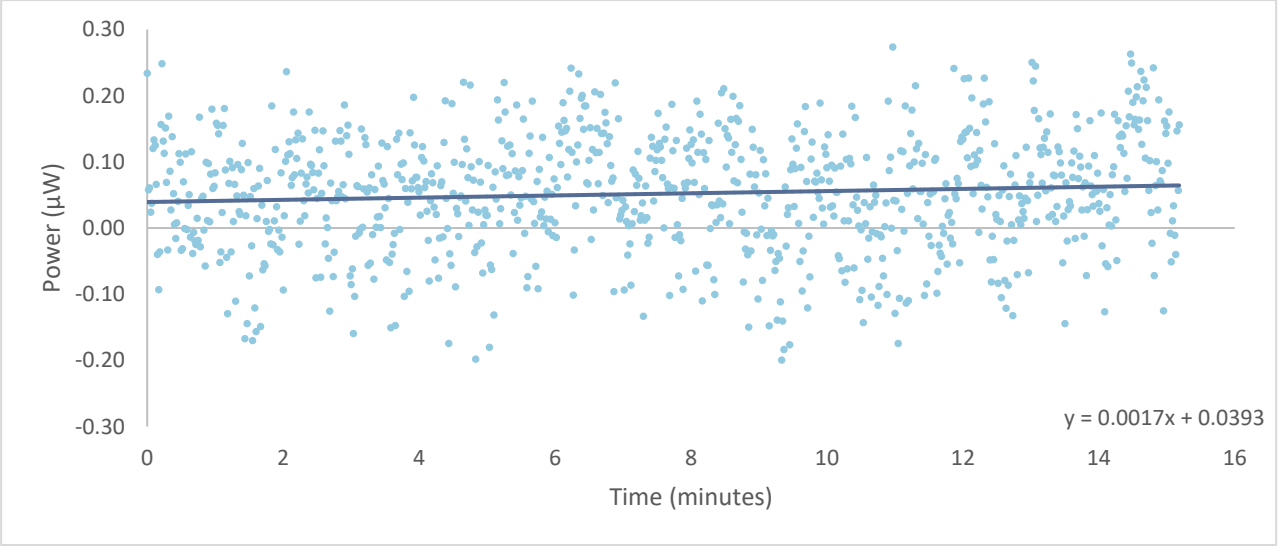

Figure C-8: Car-3, optical power transmitted in microwatts plotted against time in minutes. MF510-42 optical filter attached in set-up and cladding laying in a Carmody solution of pH 9. Linear trend line of the samples gave the function y = 0.0017x + 0.0393.

D. Statistical data

Table E-1: Summary of one-way analysis of variance of optical power signal results in experiment Car-1.

Group	*Number of samples*	*Sum*	*Average value*	*Variance*
Air	2521	16607.2356	6.58755875	0.00862602
pH 4	781	5171.0548	6.62106889	0.00733543
pH 5	720	4775.4854	6.63261861	0.00867061
pH 6	680	4505.8883	6.62630632	0.00832957
pH 7	816	5414.7012	6.63566324	0.00853746
pH 8	684	4541.4472	6.63954269	0.00821071
pH 9	812	5398.1695	6.647992	0.00860257

Table E-2: One-way analysis of variance of optical power signal results in experiment Car-1, on a 5 % significance level.

Source of variance	*Sum of squares*	*Degrees of freedom*	*Mean sum of square*	*F-observed*	*P-value*	*F-critical*
Between groups	3.843594	6	0.640599	76.2190832	1.4728E-92	2.09988484
Within groups	58.8917762	7007	0.00840471			
In total	62.7353702	7013				

Table E-3: Summary of two-tailed t-test results for Car-1 with significance level of 0.05.

Comparing groups	Two-tailed t-test result	Significantly different when significance level = 0.05?
pH 4 – pH 5	0.01272	Yes
pH 4 – pH 6	0.2604	No
pH 4 – pH 7	0.001078	Yes
pH 4 – pH 8	0.00006412	Yes
pH 4 – pH 9	2.1336E-09	Yes
pH 4 – air	3.0444E-20	Yes
pH 5 – pH 6	0.2008	No
pH 5 – pH 7	0.5209	No
pH 5 – pH 8	0.1585	No
pH 5 – pH 9	0.001256	Yes
pH 5 – air	6.62185E-30	Yes
pH 6 – pH 7	0.05004	No
pH 6 – pH 8	0.007281	Yes
pH 6 – pH 9	6.34653E-06	Yes
pH 6 – air	6.6263E-22	Yes
pH 7 – pH 8	0.4140	No
pH 7 – pH 9	0.007289	Yes
pH 7 – air	4.62882E-37	Yes
pH 8 – pH 9	0.07629	No
pH 8 – air	5.81789E-38	Yes
pH 9 – air	2.01181E-56	Yes

Table E-4: Summary of one-way analysis of variance of optical power signal results in experiment Car-2.

Group	*Number of samples*	*Sum*	*Average value*	*Variance*
pH 4 FB470-10	911	78,94	0,08665203	0,00784889
pH 6 FB470-10	911	81,82	0,08981339	0,00789722
pH 9 FB470-10	912	77,28	0,08473684	0,00802935

Table E-5: One-way analysis of variance of optical power signal results in experiment Car-2, on a 5 % significance level.

Source of variance	*Sum of squares*	*Degrees of freedom*	*Mean sum of square*	*F-observed*	*P-value*	*F-critical*
Between groups	0,01198007	2	0,00599004	0,75582238	0,46972245	2,9990208
Within groups	21,6436938	2731	0,00792519			
In total	21,6556739	2733				

Table E-6: Summary of one-way analysis of variance of optical power signal results in experiment Car-3.

Group	*Number of samples*	*Sum*	*Average value*	*Variance*
pH 4 MF510-42	911	33,62	0,0369045	0,00810667
pH 6 MF510-42	910	41,07	0,04513187	0,01026307
pH 9 MF510-42	912	47,28	0,05184211	0,00759046

Table E-7: One-way analysis of variance of optical power signal results in experiment Car-3, on a 5 % significance level.

Source of variance	*Sum of squares*	*Degrees of freedom*	*Mean sum of square*	*F-observed*	*P-value*	*F-critical*
Between groups	0,10203791	2	0,05101896	5,89649466	0,0027842	2,99902201
Within groups	23,6211101	2730	0,00865242			
In total	23,723148	2732				

Table E-8: Summary of two tailed t-test results for Car-3 with significance level of 0.05.

Comparing groups	Two-tailed t-test result	Significantly different when significance level = 0.05?
pH 6 – pH 9	0.1298	No
pH 6 – pH 4	0.06717	No
pH 4 – pH 9	0.000327	Yes

Table E-9: Summary of one-way analysis of variance of swelling capacity results of batch 1.

Group	*Number of samples*	*Sum*	*Average value*	*Variance*
SC pH 4	5	150.1204034	30.02408067	267.1260011
SC pH 5	5	296.4885548	59.29771095	171.0902566
SC pH 6	5	360.5620248	72.11240496	292.1429797
SC pH 7	5	386.0457827	77.20915655	147.468646
SC pH 8	5	373.6965683	74.73931366	408.4341746
SC pH 9	5	399.4995486	79.89990972	791.8177244

Table E-10: One-way analysis of variance of swelling capacity results of batch 1, on a 5 % significance level.

Source of variance	*Sum of squares*	*Degrees of freedom*	*Mean sum of square*	*F-observed*	*P-value*	*F-critical*
Between groups	8852.73248	5	1770.5465	5.11206503	0.00248383	2.62065415
Within groups	8312.31913	24	346.34663			
In total	17165.0516	29				

Table E-11: Summary of one-way analysis of variance of swelling capacity results of batch 2.

Group	*Number of samples*	*Sum*	*Average value*	*Variance*
SC pH 4	5	115.682402	23.1364804	259.863834
SC pH 5	5	218.138321	43.6276642	65.2707215
SC pH 6	5	247.674449	49.5348898	80.575649
SC pH 7	5	252.910298	50.5820595	123.097682
SC pH 8	5	250.350322	50.0700643	149.017651
SC pH 9	5	254.429293	50.8858586	91.3587286

Table E-12: One-way analysis of variance of swelling capacity results of batch 2, on a 5 % significance level.

Source of variance	*Sum of squares*	*Degrees of freedom*	*Mean sum of square*	*F-observed*	*P-value*	*F-critical*
Between groups	2955.95271	5	591.190541	4.61156501	0.00433168	2.62065415
Within groups	3076.73707	24	128.197378			
In total	6032.68977	29				

Table E-13: Summary of two tailed t-test results for swelling capacity results comparing batch 1 and batch 2, with significance level of 0.05.

Comparing SC of batch 1 and 2 in:	Two-tailed t-test result	Significantly different when significance level = 0.05?
Distilled water	0.00747215	Yes
pH 4	0.52118491	No
pH 5	0.05214281	No
pH 6	0.03088975	Yes
pH 7	0.0067856	Yes
pH 8	0.04768688	Yes
pH 9	0.08079852	No

Table E-14: Summary of two-tailed t-test results for swelling capacities in batch 1 with significance level of 0.05.

Comparing groups	Two-tailed t-test result	Significantly different when significance level = 0.05?
pH 4 – pH 5	0.01408056	Yes
pH 4 – pH 6	0.00406413	Yes
pH 4 – pH 7	0.00084094	Yes
pH 4 – pH 8	0.00489916	Yes
pH 4 – pH 9	0.00899198	Yes
pH 5 – pH 6	0.21975978	No
pH 5 – pH 7	0.05508152	No
pH 5 – pH 8	0.1893952	No
pH 5 – pH 9	0.17595053	No
pH 6 – pH 7	0.6015613	No
pH 6 – pH 8	0.8299343	No
pH 6 – pH 9	0.61122808	No
pH 7 – pH 8	0.82068462	No
pH 7 – pH 9	0.84925668	No
pH 8 – pH 9	0.74763507	No

Table E-15: Summary of two-tailed t-test results for swelling capacities in batch 2 with significance level of 0.05.

Comparing groups	Two-tailed t-test result	Significantly different when significance level = 0.05?
pH 4 – pH 5	0.03465179	Yes
pH 4 – pH 6	0.01262733	Yes
pH 4 – pH 7	0.01388828	Yes
pH 4 – pH 8	0.01764392	Yes
pH 4 – pH 9	0.01068376	Yes
pH 5 – pH 6	0.30589819	No
pH 5 – pH 7	0.29451379	No
pH 5 – pH 8	0.35785632	No
pH 5 – pH 9	0.23084656	No
pH 6 – pH 7	0.87374383	No
pH 6 – pH 8	0.93899066	No
pH 6 – pH 9	0.8235768	No
pH 7 – pH 8	0.94637276	No
pH 7 – pH 9	0.96413838	No
pH 8 – pH 9	0.9092394	No

Table E-16: Summary of one-way analysis of variance of swelling capacity results of batch 3.

Group	*Number of samples*	*Sum*	*Average value*	*Variance*
SC pH 4	3	0.83586265	0.27862088	0.04682879
SC pH 6	3	0.9388944	0.3129648	0.02491011
SC pH 8	3	0.89136315	0.29712105	0.01756145
SC pH 9	3	0.91562765	0.30520922	0.00857352

Table E-17: One-way analysis of variance of swelling capacity results of batch 3, on a 5 % significance level.

Source of variance	*Sum of squares*	*Degrees of freedom*	*Mean sum of square*	*F-observed*	*P-value*	*F-critical*
Between groups	0.00195397	3	0.00065132	0.02661887	0.99366583	4.06618055
Within groups	0.19574775	8	0.02446847			
In total	0.19770172	11				

Table E-18: Summary of one-way analysis of variance of swelling capacity results of batch 2.

Group	*Number of samples*	*Sum*	*Average value*	*Variance*
SC pH 4	4	3.32665321	0.8316633	0.03532065
SC pH 6	4	3.10260746	0.77565187	0.04950617
SC pH 8	4	3.72423914	0.93105978	0.04600281
SC pH 9	4	3.4617588	0.8654397	0.04243435

Table E-19: One-way analysis of variance of swelling capacity results of batch 2, on a 5 % significance level.

Source of variance	*Sum of squares*	*Degrees of freedom*	*Mean sum of square*	*F-observed*	*P-value*	*F-critical*
Between groups	0.05067726	3	0.01689242	0.38998112	0.76237895	3.49029482
Within groups	0.51979192	12	0.04331599			
In total	0.57046918	15				

Table E-20: Summary of two-tailed t-test results for average swelling capacities in batch 3 and 4 with significance level of 0.05.

Comparing groups	Two-tailed t-test result	Significantly different when significance level = 0.05?
Average SC batch 3 - Average SC batch 4	0.00047741	Yes

E. pH measurements

The pH-values of the Carmody pH-solutions were calculated from measurements of electric potential in millivolts (mV). The measurements were conducted on a JENCO 6230M pH-meter. The pH-values were calculated from measurements on mV-AUTOLOCK mode of the Carmody solutions and calibration solutions A and C of pH 4.01 and 10.04, respectively. Equation 1 was used for the pH-calculations. Calibration solution B (pH 7) was used to check the accuracy. The percent deviation of calibration solution B was calculated to be 2 and 1 % based on the values in the second and third column of table F-1, respectively.

$$C_{pH} + (X_{mV} - C_{mV}) * \frac{A_{pH} - C_{pH}}{A_{mV} - C_{mV}} \quad (1)$$

Table F-1: Electric potential (mV) for calibration solutions.

Calibration solution	Electric potential (mV)	Electric potential (mV)
A	161	158
B	-179	-175
C	-15	-12

The second column of table F-1 was measured for the calculations of the pH-values of the Carmody solutions used in experiments Car-1 to Car-3. The third column was measured on another day for the calculations of the Carmody solutions used in the swelling capacity experiments.

Table F-2: Electric potential (mV) and calculated pH-values of Carmody solutions

Carmody solutions used in:	**Car-1, Car-2, Car-3**		**Batches 1-2 SC experiments**		**Batches 3-4 SC experiments**	
	Electric potential (mV)	Calculated pH	Electric potential (mV)	Calculated pH	Electric potential (mV)	Calculated pH
pH 4	187	3.55	185	3.58	174	3.78
pH 5	135	4.47	134	4.49		
pH 6	82	5.41	81	5.43	80	5.45
pH 7	21	6.49	22	6.48		
pH 8	-23	7.27	-20	7.22	-11	7.06
pH 9	-92	8.50	-88	8.43	-80	8.28